AD A123501

Sponsored by
Advanced Research Projects Agency (DOD)
ARPA Order No. 3291

ARPA Order 3291
Program Code 7F10
Name of Grantee: University of Colorado
Effective Date of Grant: 1 November 1974
Grant Expiration Date: 31 October 1976
Amount of Grant: $173,016
Grant Number: AFOSR-75-2775
Principal Investigator: Carl Kisslinger (303) 492-7943
Program Manager: William J. Best
Title of Work: Seismic Wave Propagation and Earthquake Characteristics in Asia

Semi-Annual Technical Report No. 4
1 May 1976 - 31 October 1976
C. Kisslinger, E.R. Engdahl, M. Wyss
W. Gawthrop, G. Lundquist

DTIC FILE COPY

DTIC
ELECTE
JAN 18 1983
S D
D

83 01 17 151

Best
Available
Copy

APPROVED FOR PUBLIC RELEASE: DISTRIBUTION UNLIMITED.

Table of Contents

Accession For	
NTIS GRA&I	☒
DTIC TAB	☐
Unannounced	☐
Justification	
By	
Distribution/	
Availability Codes	
Dist	Avail and/or Special
A	

DTIC COPY INSPECTED 2

Technical Report Summary

1. The great influence of the way in which inelastic attenuation is modelled on the results obtained for seismic source parameters from wave spectra has led to an investigation of better ways of arriving at the required corrections to raw seismogram spectra. A procedure, based on a relaxation model of attenuation, for using a frequency-dependent Q in the program for computing source spectra has been developed. The resulting effective Q's tie together apparently disparate results obtained by others for short-and long-period attenuation. Moments and corner frequencies for 12 central Asian earthquakes in four selected seismic zones in western China and Siberia have been determined from P- and S-body wave spectra. The range of calculated moments is 10^{23} to 10^{26} dyne-centimeters. The corner frequencies from P-wave spectra decrease with increasing moment in a way that is at least qualitatively as expected. However, the S-wave corner frequencies are found to be independent of moment for this small sample of events, a result that calls for further consideration of the validity of the analysis.

2. The computation of seismic source parameters from the properties of the seismic signal, expressed in either the time-domain or frequency domain, depends on the investigator's choice of source model from among several competing ones. An opportunity to test competing models empirically is, therefore, of great value. The Haicheng, China, earthquake of February 4, 1975 is the only Asian earthquake for which we have detailed information about source parameters from on-site geodetic measurements and aftershock locations based on a local network. We are using these local data to calibrate techniques for determining the same source properties from teleseismic data. The data have been screened for quality and the spectra are being computed. The

waveforms will be compared with synthetic seismograms calculated on the basis of Archambeau's source theory.

3. Previous work under this grant by Boucher and Herrmann has led to the development of a technique for estimating focal depth and focal mechanism of crustal events from synthesized long-period seismograms. An attempt has been made to automate the Herrmann technique, but the program is not yet operational because of the existence of secondary maxima in the correlation coefficients used, such that the program will sometimes find one of these and select a wrong answer.

The resolution and accuracy of the technique depends on the adequacy of the models selected for source and receiver crustal structures. A program has been developed that uses data from earthquakes recorded on a local network to simultaneously locate the set of earthquakes and fix a crustal model. The model always incorporates a linear increase of velocity with depth in the crust. The parameters calculated by the generalized inversion procedure are the thickness of the crust, the surface velocity, the rate of increase of velocity with depth in the crust, and the Pn velocity. For those places at which the required data are available, this program will yield results that will improve significantly the output of the focal parameter procedure.

1. Spectral Classification of Asian Seismic Events

Gary Lundquist

Introduction.

We have used averaged seismic source spectra to determine both seismic source parameters and transmission properties of the Earth. Though each estimation involved assumptions about the other, we feel that, by varying parameters and drawing upon externally derived theories, unknowns in both the source and transmission may be estimated.

The computation of the source spectra involved several stages. In the first stage, smoothed autospectra were computed for the available seismograms of 12 central Asian earthquakes, 3 in each of the 4 geological provinces previously selected for study. Semi-annual report No. 2 of October, 1975, described the computation procedure. At that time, stations with bad signal-to-noise ratio were dropped from further processing, though some borderline cases were retained. In the second stage, initial corrections were made to the seismogram spectra, including instrumental response, geometric attenuation (or spreading), crustal response, acoustic impedance contrast, and anelastic attenuation. We considered the correction for radiation pattern and concluded that such a correction was inappropriate for crustal earthquakes. First, pP and sP were also in the time window, and we would have been correcting the energy transported by those phases with a perhaps significantly different radiation pattern computed for direct P. In addition, we have found accurate focal mechanisms difficult to determine. The events are small; station distribution is not optimum, and the adopted take-off-angles from the source are almost certainly in error due to complexities in the crust.

Once initial corrections had been made, the next step was to examine the adequacy of some of those corrections. In the case of the spreading correction, we found evidence of consistent undercorrection of near stations. That is,

some travel paths in the 10-25° range in central Asia suffer much more rapid spreading than paths in an average Earth model. The effect of this under-correction is to cause a spread in levels of individual station spectra, and to make the seismic moments slightly lower for those events which rely on near stations. The shape of the averaged spectra will not be dominated by one high level station, however, since we employ a logarithmic average rather than an RMS average. The interpretation of the evidence on spreading will require further study, and should probably be combined with a ray tracing experiment.

The investigation of the inadequacy of standard anelastic attenuation models shows more immediate results in terms of Earth properties and is the subject of the first major section of this chapter. Briefly, we found a range of models available, some derived from surface waves and others for high-frequency body waves. Rather than discard any model, we have generated a modulation of attenuation based upon the relaxation theory of dissipation mechanisms which resolves the differences between models.

Finally, we went back to the raw spectra and computed station spectra employing the corrections that we felt were the best available. Those spectra and their interpretation are the subjects of the second part of this chapter. The consistency of magnitude-moment curves and moment-corner frequency graphs provide checks on the computation and correction techniques used.

The anelastic attenuation of seismic body-waves.

Our treatment of anelastic attenuation began with the basic assumption that the specific quality factor, Q^{-1}, was not frequency-independent. This decision stemmed from the differences between two California Institute of Technology models. CIT 208 was derived from short-period body waves, and for

shallow earthquakes could be represented by a constant T/Q_{eff} ratio of ~ 0.45, where T is travel time and Q_{eff} is Q integrated over the travel path. CIT 11CS2-QM, on the other hand, was determined from surface wave data and gave $T/Q_{eff} \sim 1.0$. The discrepancy between the T/Q_{eff} ratios could imply an error in one model, but we have chosen to accept both as correct, and to take Q^{-1} is frequency dependent.

We may write the energy of a harmonic wave in terms of its initial value, $E_o(\omega)$ and a spreading factor $G(x)$, as (Anderson, 1967)

$$E(\omega) = GE_o(\omega)\, e^{2i(\kappa x - \omega t)} \tag{1.1}$$

where κ is a complex wave number, $\kappa = \kappa' + i\kappa''$. The specific quality factor, Q^{-1}, is defined as the fraction of energy dissipated per wavelength. If the energy loss is small, then to first order the energy carried is given by (1.1). Neglecting common factors,

$$Q^{-1} = \frac{1}{2\pi}\frac{\Delta E}{E}$$

$$= \frac{1}{2\pi}\frac{e^{-2\kappa''x}\, e^{2i(\kappa' - \omega t)} - e^{-2\kappa''(x + 1/\kappa')}\, e^{2i[\kappa'(x + 1/\kappa') - \omega t]}}{e^{-2\kappa''x}\, e^{2i(\kappa' x - \omega t)}}$$

$$= 1 - e^{-2\kappa''/\kappa'} \tag{1.2}$$

For small κ'', the series expansion of an exponential gives

$$Q^{-1} = \frac{2\kappa''}{\kappa'} \tag{1.3}$$

We may distinguish between P-wave and S-wave attenuation by writing the respective wave numbers in terms of complex velocities.

$$\kappa_\alpha^2 = \frac{\omega^2}{\alpha^2} = \frac{\omega^2}{1/\rho(k + 4/3\mu)}$$

$$\kappa_\beta^2 = \frac{\omega^2}{\beta^2} = \frac{\omega^2}{\mu/\rho} \qquad (1.4)$$

where k and μ are complex bulk and shear moduli, respectively. For the case of small attenuation,

$$Q_\alpha^{-1} = \frac{k'' + 4/3\mu''}{k' + 4/3\mu'}$$

$$Q_\beta^{-1} = \frac{\mu''}{\mu'} \qquad (1.5)$$

Equations (1.5) give the explicit dependence of anelastic attenuation on the imaginary parts of the elastic moduli. It is important to note that both P and S waves suffer attenuation from shear mechanisms ($\mu'' \neq 0$), but P waves may suffer additional attenuation from bulk losses ($k'' \neq 0$). In assuming Q^{-1} is a function of frequency, we are assuming that μ'' and k'' are frequency dependent. Bulk losses are generally assumed to be small, and setting $k'' = 0$ in (1.5) gives

$$\frac{Q_\alpha^{-1}}{Q_\beta^{-1}} = \frac{4}{3}\left(\frac{\beta}{\alpha}\right)^2 \qquad (1.6)$$

so that, $\frac{Q_\alpha}{Q_\beta} = 2.25$ for Poisson's ratio = 0.25. If $\left.\frac{T}{Q_{eff}}\right|_\alpha = 1.0$, then (1.6) implies $\left.\frac{T}{Q_{eff}}\right|_\beta \sim 4.0$.

We will relate these definitions of Q^{-1} to relaxation phenomena through the "standard linear elastic solid" model (Mason, 1958). The model may be visualized as a spring of stiffness, M_1, in series with a parallel combination of dashpot (viscosity η_2) and spring (stiffness M_2). At high

frequencies, or upon sudden application of a stress, the system has an instantaneous elastic response controlled by M_1 , the unrelaxed system elastic modulus. At very low frequencies, or upon application of a constant stress, the system modulus is the relaxed stiffness of the series springs,

$$M_R = \frac{M_1 M_2}{M_1+M_2}$$

The anelastic dashpot controls the frequency range over which the change in modulus goes from M_1 to M_R , and therefore the frequency band over which absorption takes place.

For a harmonic stress, the stress-strain relation is (Liu et al., 1976).

$$\sigma + \tau_\sigma \dot{\sigma} = M_R(\varepsilon+T_\varepsilon \dot{\varepsilon}) \qquad (1.7)$$

where $\tau_\sigma = \eta_2/(M_1 + M_2)$ is the stress relaxation time for constant strain, and $\tau_\varepsilon = \eta_2/M_2$ is the strain relaxation time for constant stress. Since

$$\dot{\sigma} = \frac{\partial \sigma}{\partial t} = j\omega\sigma$$

and

$$\dot{\varepsilon} = \frac{\partial \varepsilon}{\partial t} = j\omega\varepsilon$$

then

$$\sigma(1 + j\omega\tau_\sigma) = M_R(1 + j\omega\tau_\varepsilon)\varepsilon \qquad (1.8)$$

Thus we obtain the complex modulus as

$$\frac{\sigma}{\varepsilon} = M_C = M_R \left(\frac{1 + j\omega\tau_\sigma}{1 + j\omega\tau_\varepsilon} \right)$$

$$= M_R \left[\frac{1 + \omega^2 \tau_\sigma \tau_\varepsilon + j\omega(\tau_\sigma - \tau_\varepsilon)}{1 + \omega^2 \tau_\varepsilon^2} \right] \qquad (1.9)$$

We can now use (1.5) to define Q^{-1} as the ratio of the imaginary part of M_C to the real part.

$$Q^{-1} = \frac{\omega(\tau_\varepsilon - \tau_\varepsilon)}{1 + \omega^2 \tau_\sigma \tau_\varepsilon}$$

$$= C(M_1, M_2) \left[\frac{\omega\tau}{1 + \omega^2 \tau^2} \right] \qquad (1.10)$$

where $\tau = \sqrt{\tau_\sigma \tau_\varepsilon}$ is the average system relaxation time, and $C(M_1, M_2)$ is a constant depending upon the elastic moduli of the system. In (1.10) we have isolated the frequency dependent behavior inside the square brackets. That factor, which we call $R(\omega)$, gives a bell-shaped graph of Q^{-1} vs. frequency.

The above are all well known results, and any medium which may be modelled as a standard linear solid will show absorption over a limited frequency band and appear elastic at other frequencies, though different elastic moduli apply. The Earth is much more complex than this standard solid however, and such a model applies only over limited frequency ranges. Liu *et al*, (1976), however, believe the model can be applied about relaxation times so closely spaced that the various absorption bands overlap, and Q^{-1} is essentially constant. This requires frequent changes in the imaginary elastic moduli, and many mechanisms have been described which will give the required spectrum of relaxation time, and an essentially frequency independent Q^{-1}.

The application of anelastic attenuation correction based on the constant T/Q_{eff} ratios implied by (1.6), however, leads to inconsistencies. Conservation of energy requires that amplitude spectra must decay at least as fast as $\omega^{-3/2}$ at high frequencies. And interference under Huyghen's principle indicates that the decay should occur when wavelengths are on the order of fault size or smaller, implying a corner frequency well within the passband of WWSSN seismographs. Also, the shortest time constant of rupture is probably on the order of the rise time or smaller, implying smooth or continuous acceleration to frequencies greater than the inverse of the rise time. Those frequencies should also be in the passband of WWSSN short-period instruments, and should decay at least as fast as ω^{-3}. Observed slopes at high frequencies after initial corrections were positive, rather than negative, especially for S-wave spectra, implying an error in the correction technique.

The total anelastic attenuation correction is given by

$$e^{\frac{\omega T}{2Q_{eff}}} \tag{1.11}$$

The slope of the corrected spectrum is affected by either changing T/Q_{eff} or making Q_{eff}^{-1} a function of frequency. We have chosen the latter, and modulate Q^{-1} according to

$$\begin{aligned} Q^{-1}(z, \omega) &= Q^{-1}(z) \quad , \omega < \frac{1}{\tau} \\ Q^{-1}(z, \omega) &= Q^{-1}(z)\, R(\omega) \, , \omega \geq \frac{1}{\tau} \end{aligned} \tag{1.12}$$

where $R(\omega)$ is defined in (1.10). One aspect of the substitution of $R(\omega)$ into the exponent of (1.11) is the fact that Q_{eff} is an integration of Q over the travel path. According to (1.12), we have assumed $R(\omega)$ to be

of path, so that it comes out of the integration. This is obviously a simplification, and the property of path independence must be tested. In particular, we expect a different modulation for deep events.

The result of the modulation defined by (1.12) is that we model a hole in the spectrum of relaxation times. The decay in Q^{-1} has the shape of a similar decay in a linear elastic solid, with the beginning of the decay at $\omega = 1/\tau$. Figure 1.1 shows the total anelastic attenuation correction for P and S waves as a function of τ , where the unmodulated correction assumes constant T/Q_{eff} ratios of 1.0 and 4.0 for P and S waves, respectively. In Figures 1.2 to 1.5 we show spectra corrected with various τ modulations for each of our four geographic areas.

The P-wave spectra yield to simple interpretations. $\tau_\alpha = 0.3$ is adequate for all 12 events studied thus far, though events dominated by near stations could just as well use larger τ_α . The choice of τ_α is made according to the slope criterion previously discussed, and an ω^{-3} decay rate is sought. The choice of $\tau_\alpha = 0.3$ gives an acting T/Q_{eff} ratio of 1.0 at 20 sec period and 0.5 at .5 sec period, effectively combining the two CIT models using a standard elastic solid decay rate. τ_α is also path independent, so far as this study is concerned.

The interpretation of the S-wave spectra is not so simple. In this report we present the results of using $T/Q_{eff} = 4.0$, and comment on the conclusions which would have to be made if this model were correct. If the choice of τ_β were made on the basis of high frequency decay, $\tau_\beta = 0.7$ would be the minimum value. However, a subjective estimate of spectral quality leads this investigator to prefer $\tau_\beta = 1.1$. For $\tau_\beta < 1.1$, most of the S-wave spectra had definitely peaked character, and the interpretation of a long period level for seismic moment is difficult.

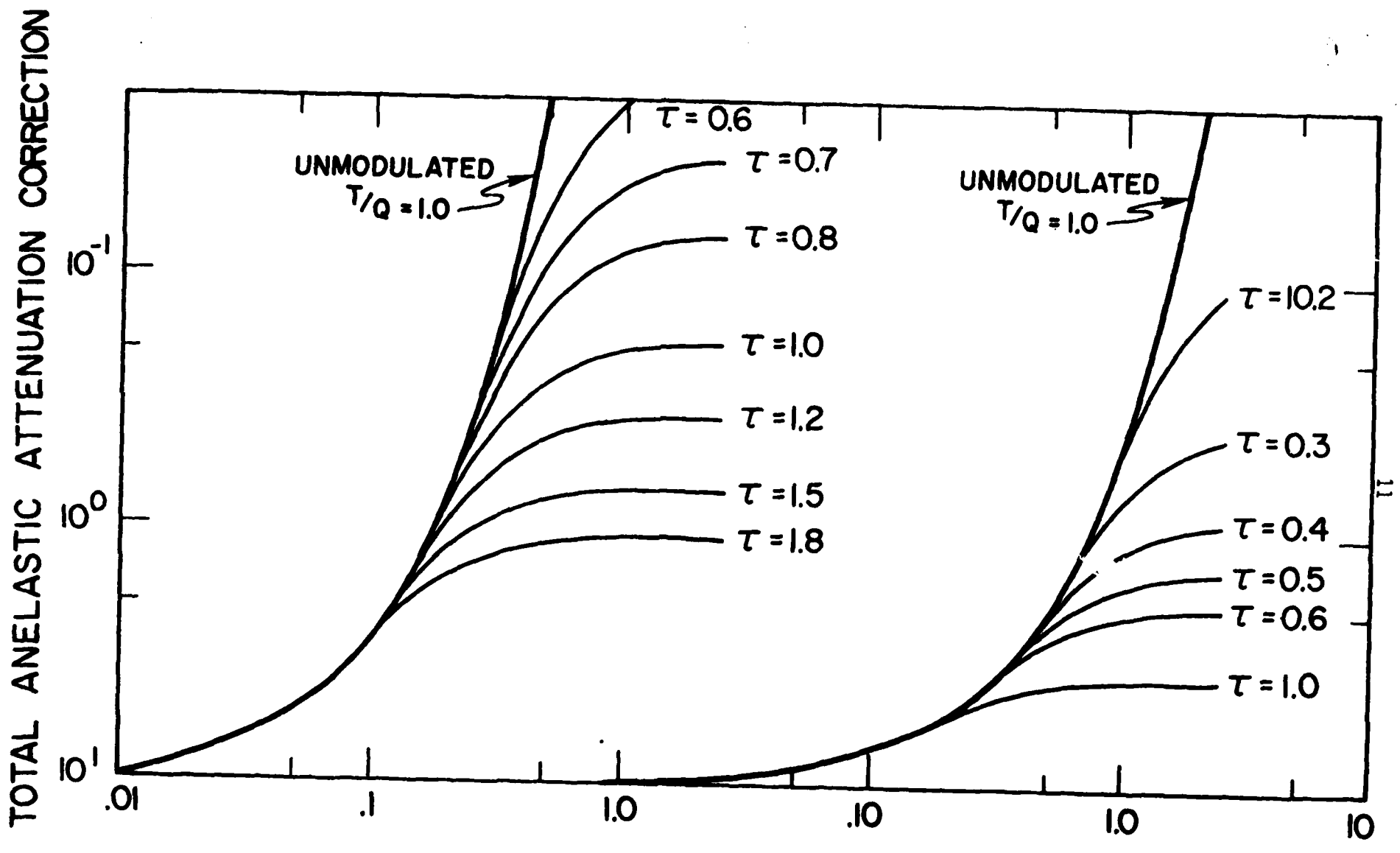

Figure 1.1: Total P and S-wave anelastic attenuation correction. is the relaxation time from a standard linear elastic solid model.

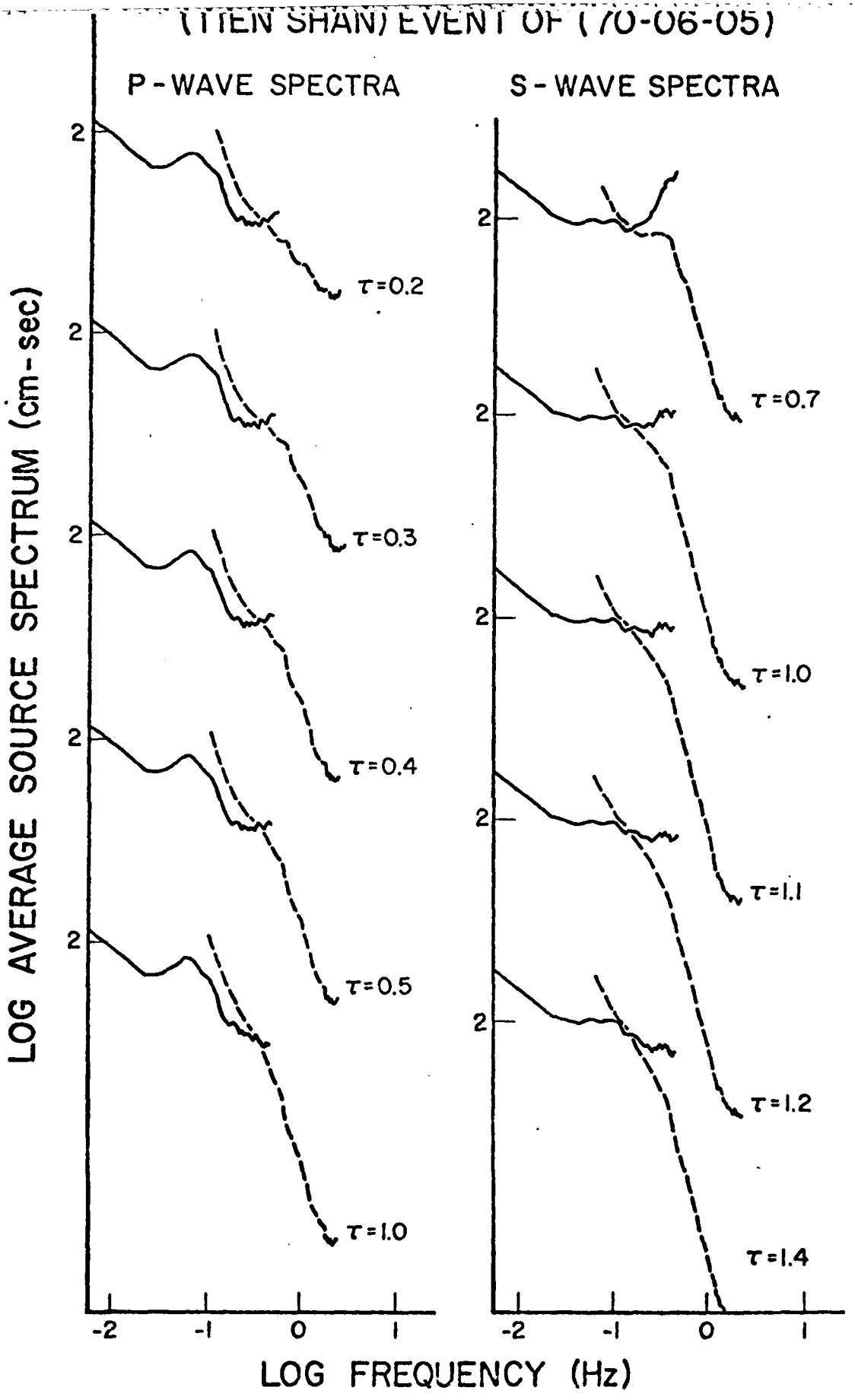

Figure 1.2: Q test as a function of τ . Tien Shan region.

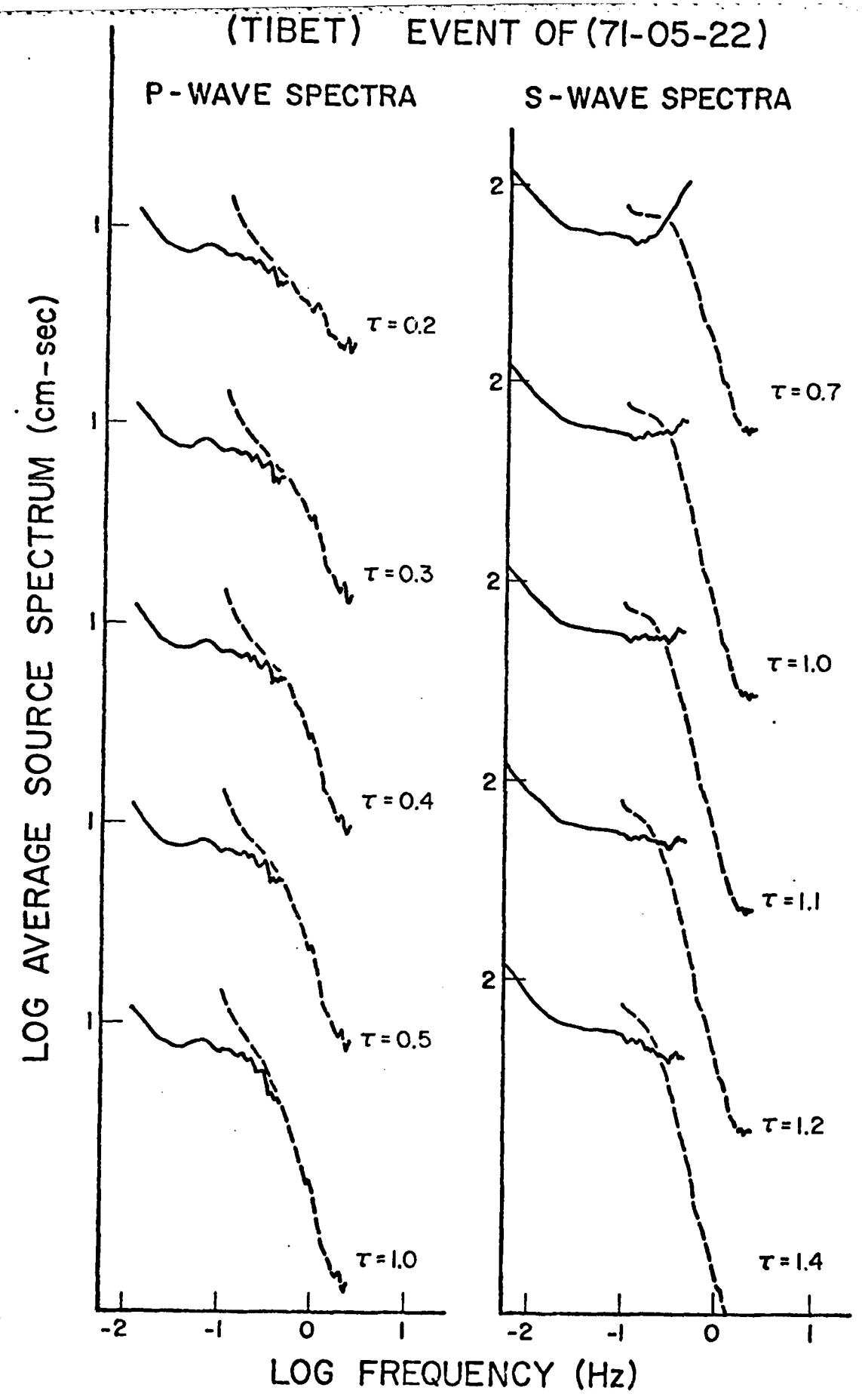

Figure 1.3: Q test as a function of τ . Tibet region.

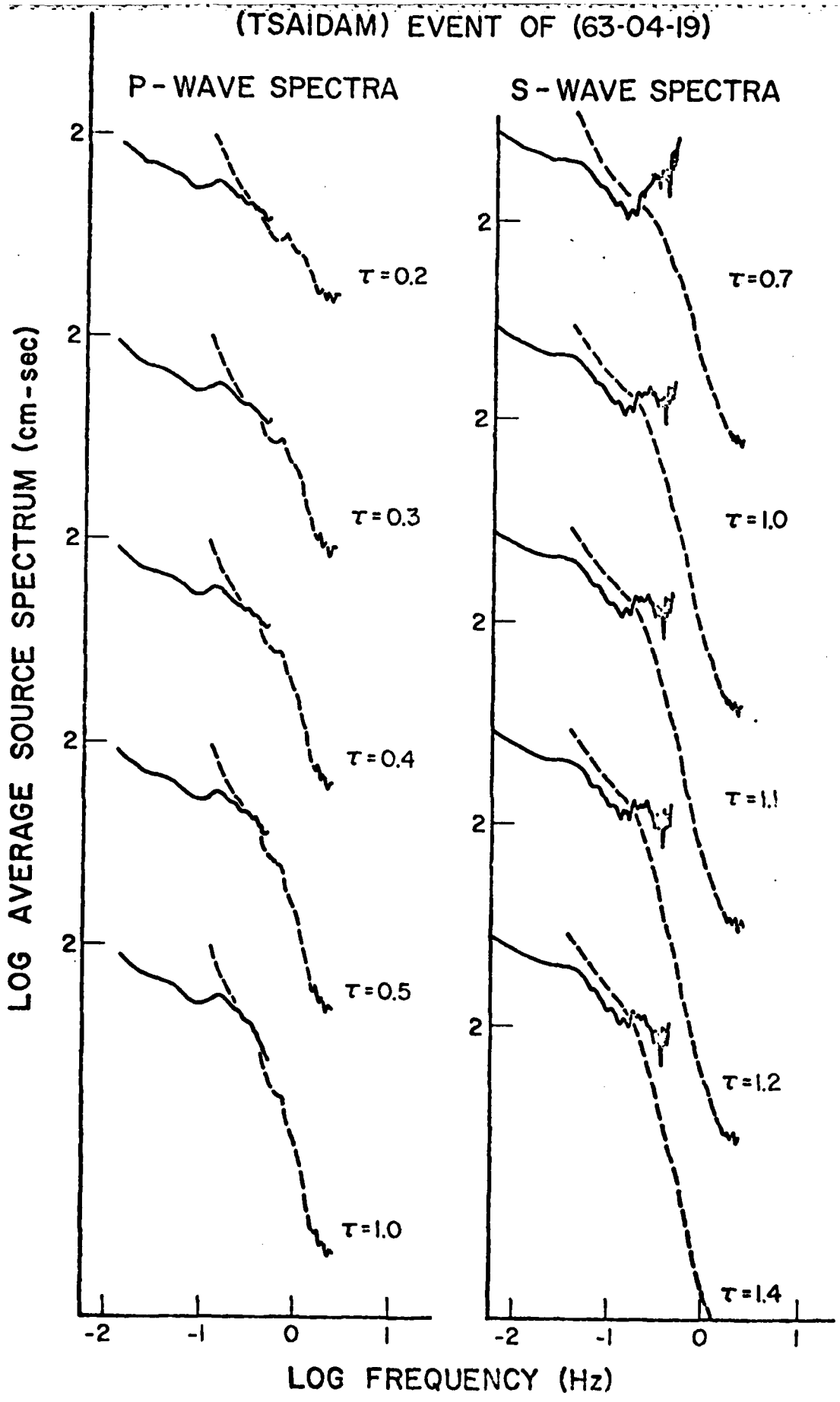

Figure 1.4: Q test as a function of τ . Tsaidam region.

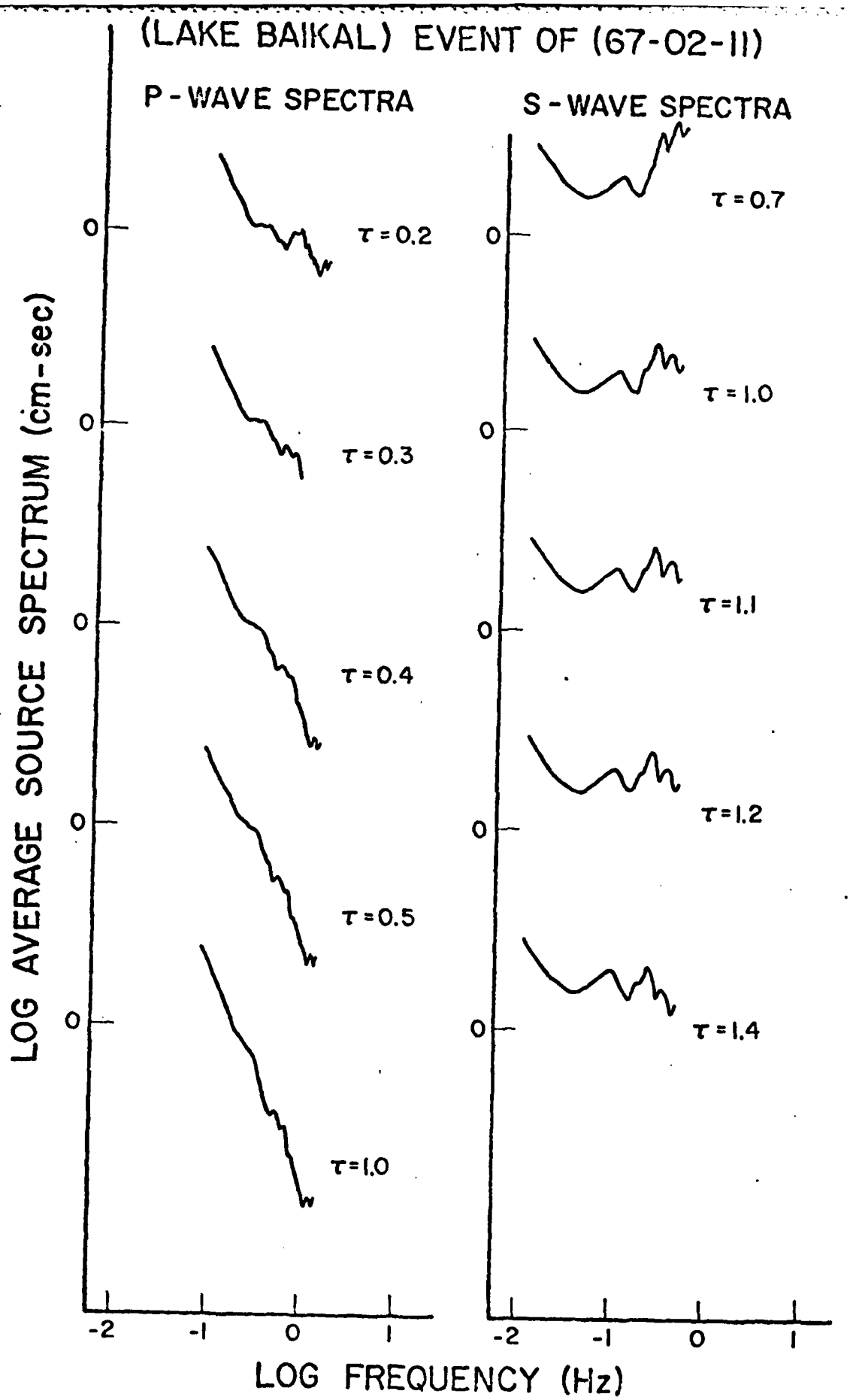

Figure 1.5: Q test as a function of τ . Lake Baikal region.

In either case, $\tau_\beta < 0.7$ does not give an acceptable slope, implying that P waves are attenuated to higher frequencies than are S waves. That is, the spectrum of relaxations which are controlled by the shear modulus has a decay toward high frequencies from a peak at about .15 Hz, while a separate dissipation mechanism operating on the bulk modulus maintains P-wave attenuation out to .5 Hz. The half amplitude points for Q_β^{-1} and Q_α^{-1} are at about 0.5 and 2 Hz, respectively, for $\tau_\beta = 1.1$ and $\tau_\alpha = 0.3$ sec. If $\tau_\beta = 0.7$, the peak would be at .2 Hz and the half amplitude at .7 Hz. The range of acceptable τ_β never permits a complete overlap of the P and S attenuation spectra. Figure 1.6 diagrams these results on a log-log graph.

Two bulk loss mechanisms have been studied in the literature. Biot (1956, 1956a) studied the propagation of stress waves in a saturated porous solid. In his model, the pores were interconnected, and a compressible fluid was allowed to move with respect to the solid matrix. His results show peaked attenuation, with Q^{-1} decaying as $\omega^{-\frac{1}{2}}$ at high frequencies. The location of the peak depends in a complex way upon fluid viscosity, velocity and density, the frictional forces on the fluid, the pore (tube) diameter and length and the mathematical model of flow. There is sufficient flexibility in his parameterizations that such a mechanism could be called upon to explain the observed P wave attenuation peak. However, the decay as only $\omega^{-\frac{1}{2}}$ would require a different choice of τ_α, a test which has not been made.

The second possible bulk loss mechanism was examined by Vaisnys (1968). He proposes that a material which is in equilibrium very near its melting point may change phase under stress. And if the stress is harmonic, the entropy production would vary with frequency, being peaked for frequencies about $1/\tau$, the characteristic rate constant of the process. Essentially, the medium would

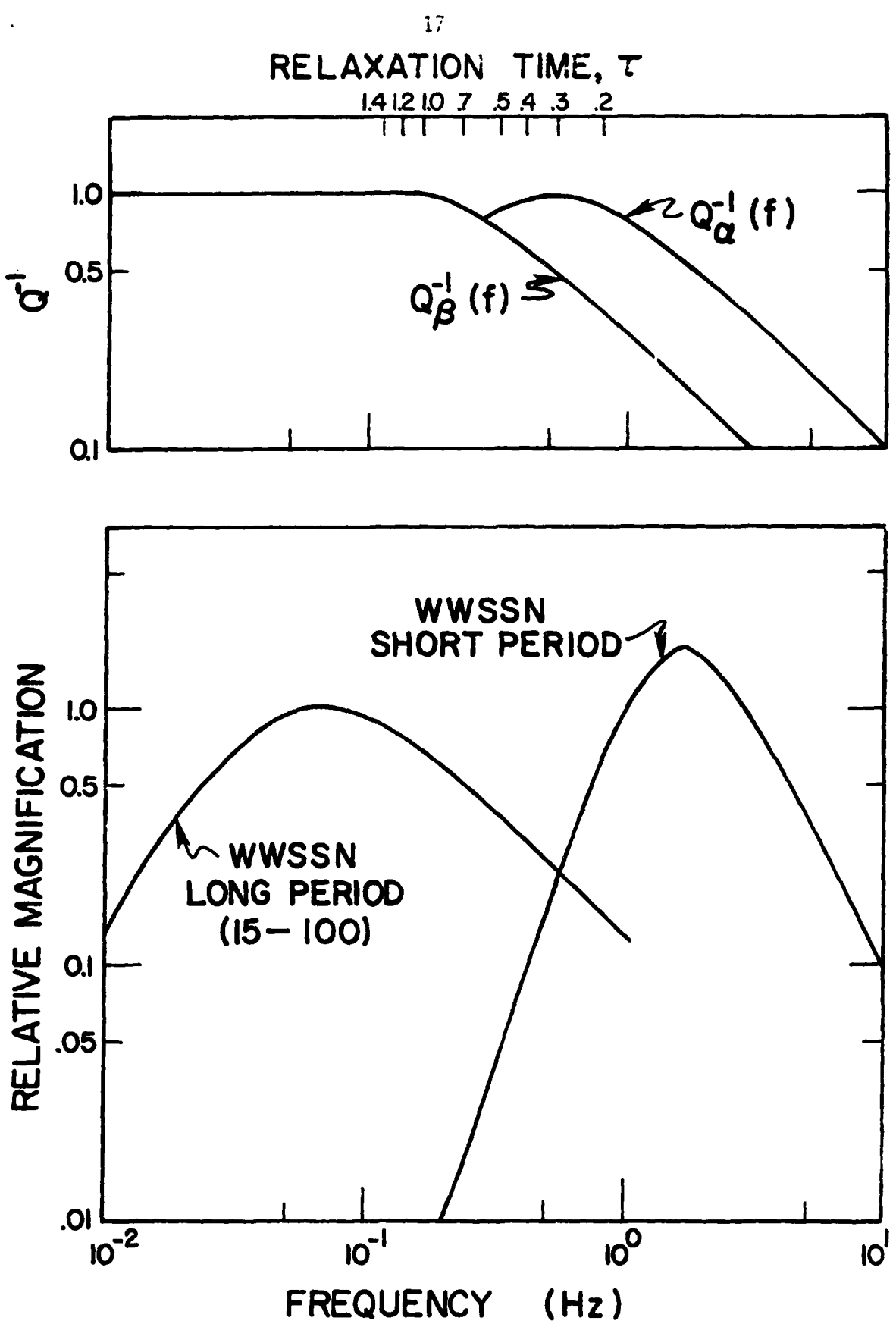

Figure 1.6: The frequency dependent corrections to the seismogram spectra. At the bottom are the instrument responses for WWSSN seismographs. At the top Q^{-1} is plotted vs. frequency for [illegible] 1.1 and 0.3.

tend to freeze during one half cycle, then thaw during the other half cycle. Since more energy is required to order a lattice than to disorder a lattice, the effect would be a slightly greater fraction of melt after the wave has passed. Since this mechanism requires pressure changes, it would attenuate only P waves.

Vaisnys examines three cases: (1) an ideal solution partial melt; (2) solid in equilibrium with its own melt; and (3) solid-solid phase transformation. For each he finds attenuation to be peaked in exactly the form we have described for a standard linear solid. The relaxation times are 10 sec, 90 sec and greater than 10^3 sec, respectively. Thus all time constants are greater than $\tau_\alpha = 0.3$ as observed here. However, though the thermodynamic character of the medium is completely parameterized, Vaisnys makes no effort to compare those properties to upper mantle properties. Thus this mechanism might also apply.

We state again, that the separation of distinct P and S attenuation mechanisms relies upon both our choice of τ and T/Q_{eff}. We will see in the next section that our choice of parameters for S is likely in error, since corner frequencies tend to concentrate around .25-.3 Hz, independent of the size of the events. Also, while P wave spectra sometimes appear to be two cornered, the S wave spectra rarely are. Thus there is good reason to question the validity of the choice of parameters for S and, perhaps, of the whole concept. This writer feels the beauty of the relaxation concept of specific dissipation mechanisms as well as the consistency of the P wave results justify the present effort, as well as further work.

Presentation of spectra.

Average seismic body-wave spectra are presented in Figures 1.7 to 1.18, with three earthquakes studies in each of (1) the Tien Shan fold belt; (2) the

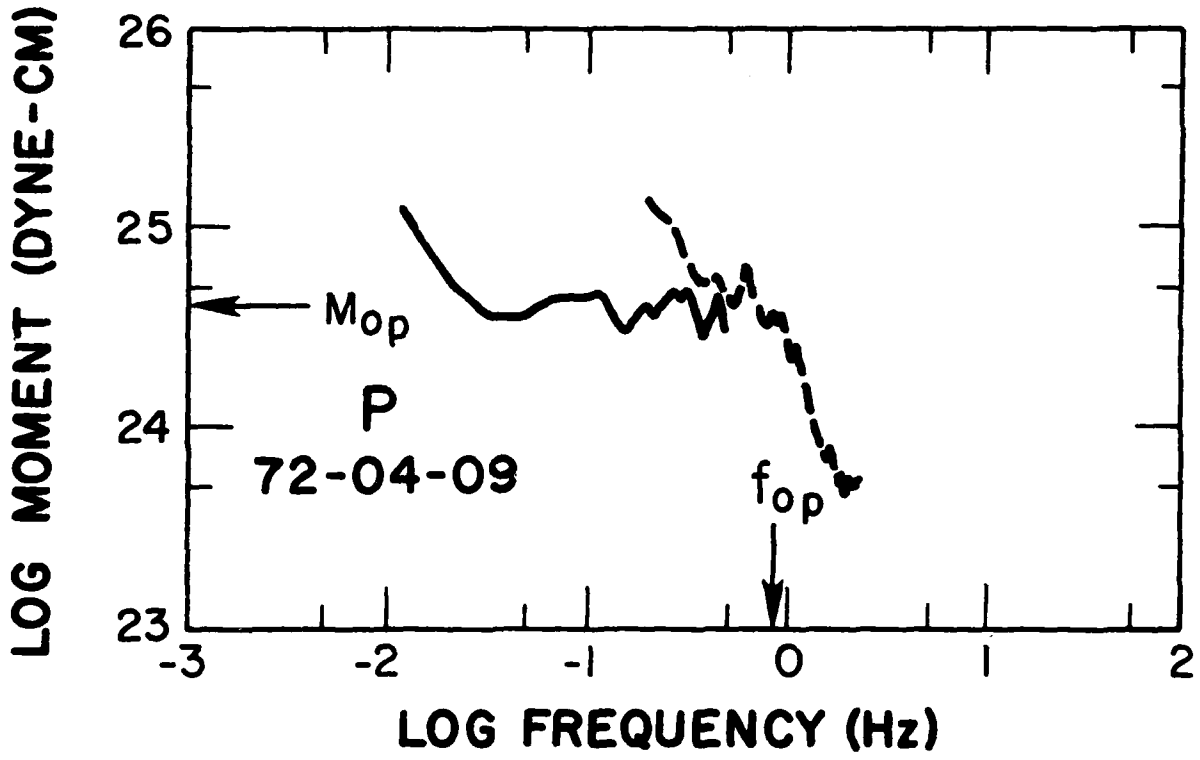

Figure 1.7: Average source spectrum, Tien Shan event of 72-04-09. SPP from 7, LPP from 7.

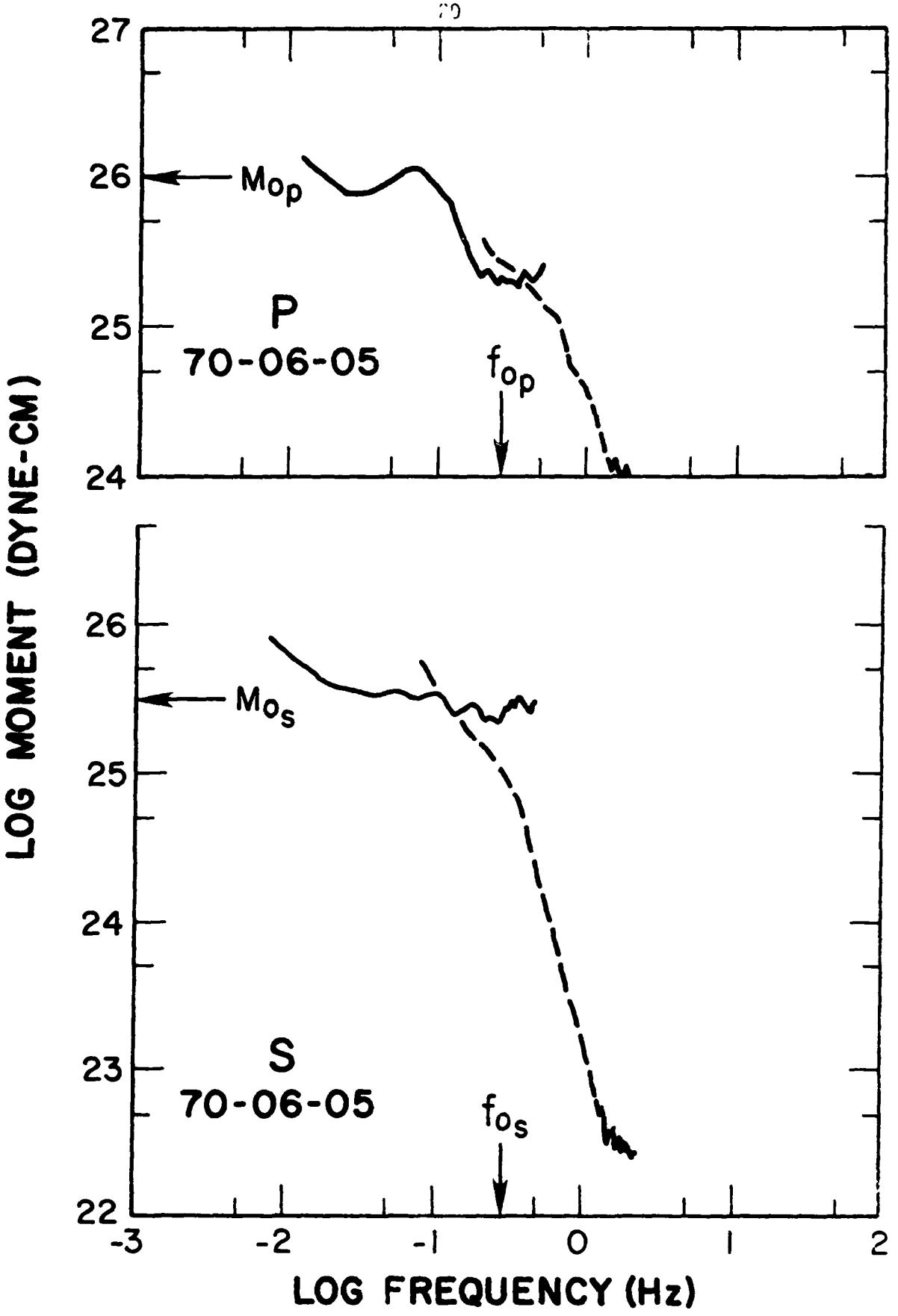

Figure 1.8: Average source spectrum, Tien Shan event of 70-06-05. SPP from 9, LPP from 7, SPS from 8, LPS from 9.

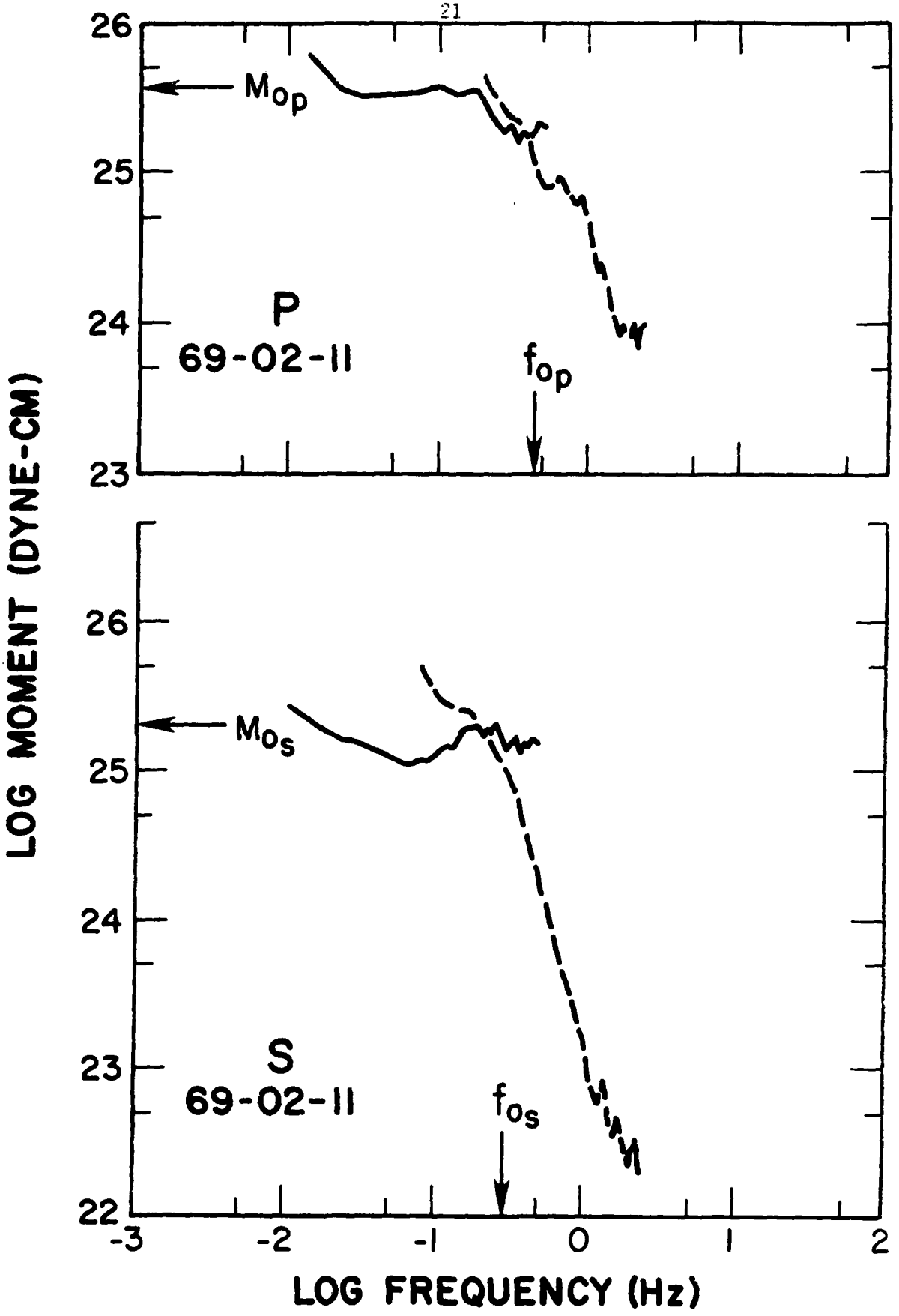

Figure 1.9: Average source spectrum, Tien Shan event of 69-02-11. SPP from 5, LPP from 7, SPS from 3, LPS from 5.

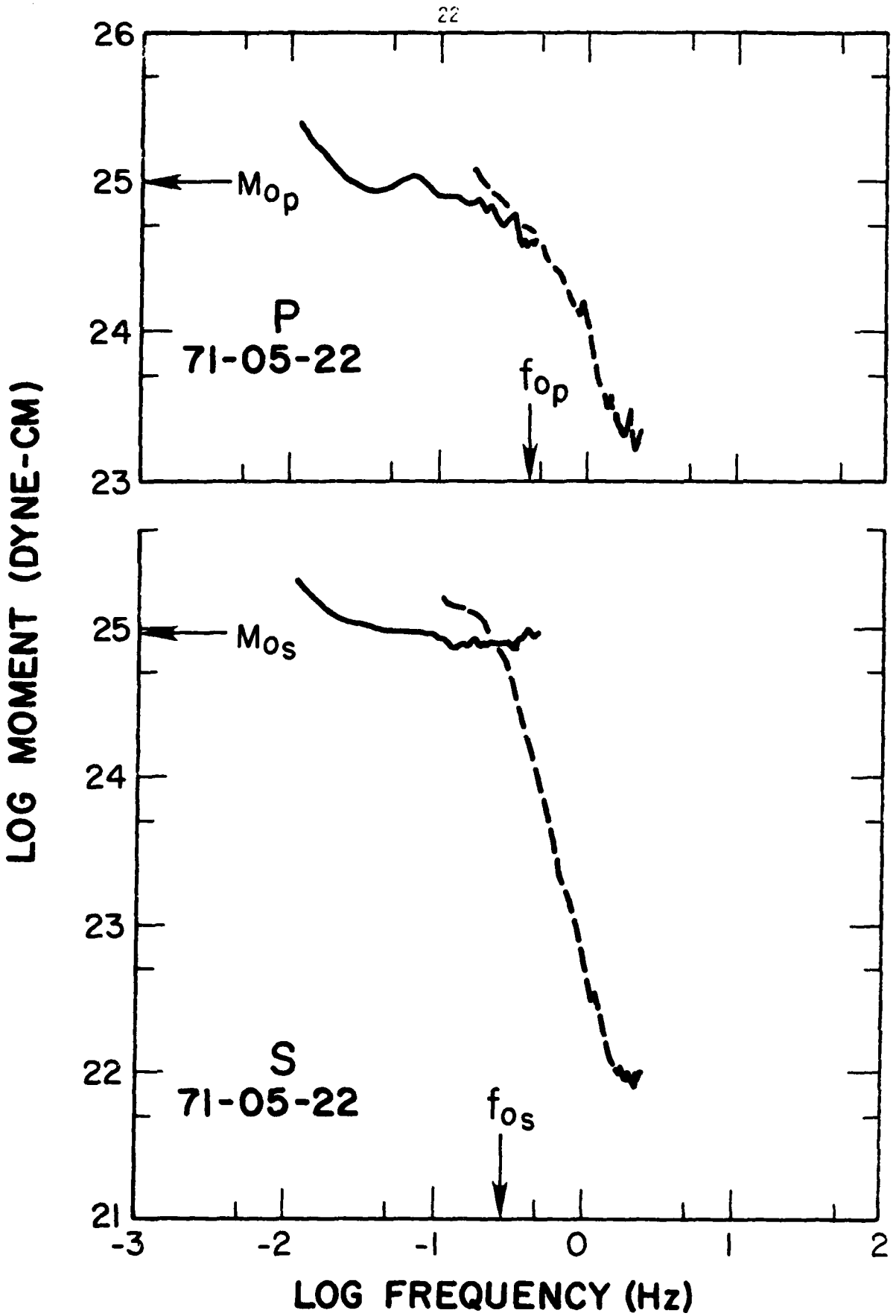

Figure 1.10: Average source spectrum, Tibet event of 71-05-22. SPP from 7, LPP from 5, SPS from 5, LPS from 9.

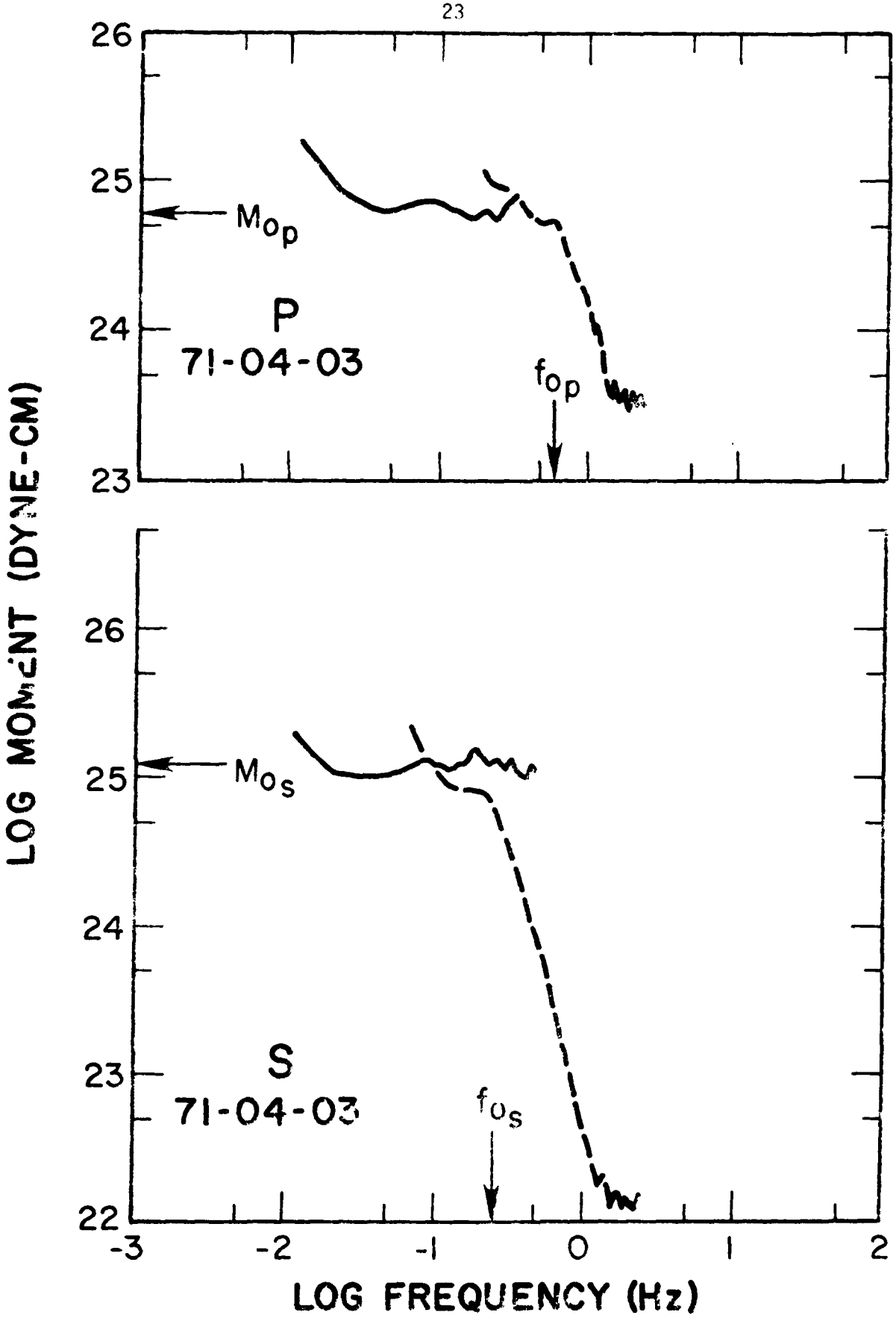

Figure 1.11: Average source spectrum, Tibet event of 71-04-03. SPP from 10, LPP from 4, SPS from 4, LPS from 9.

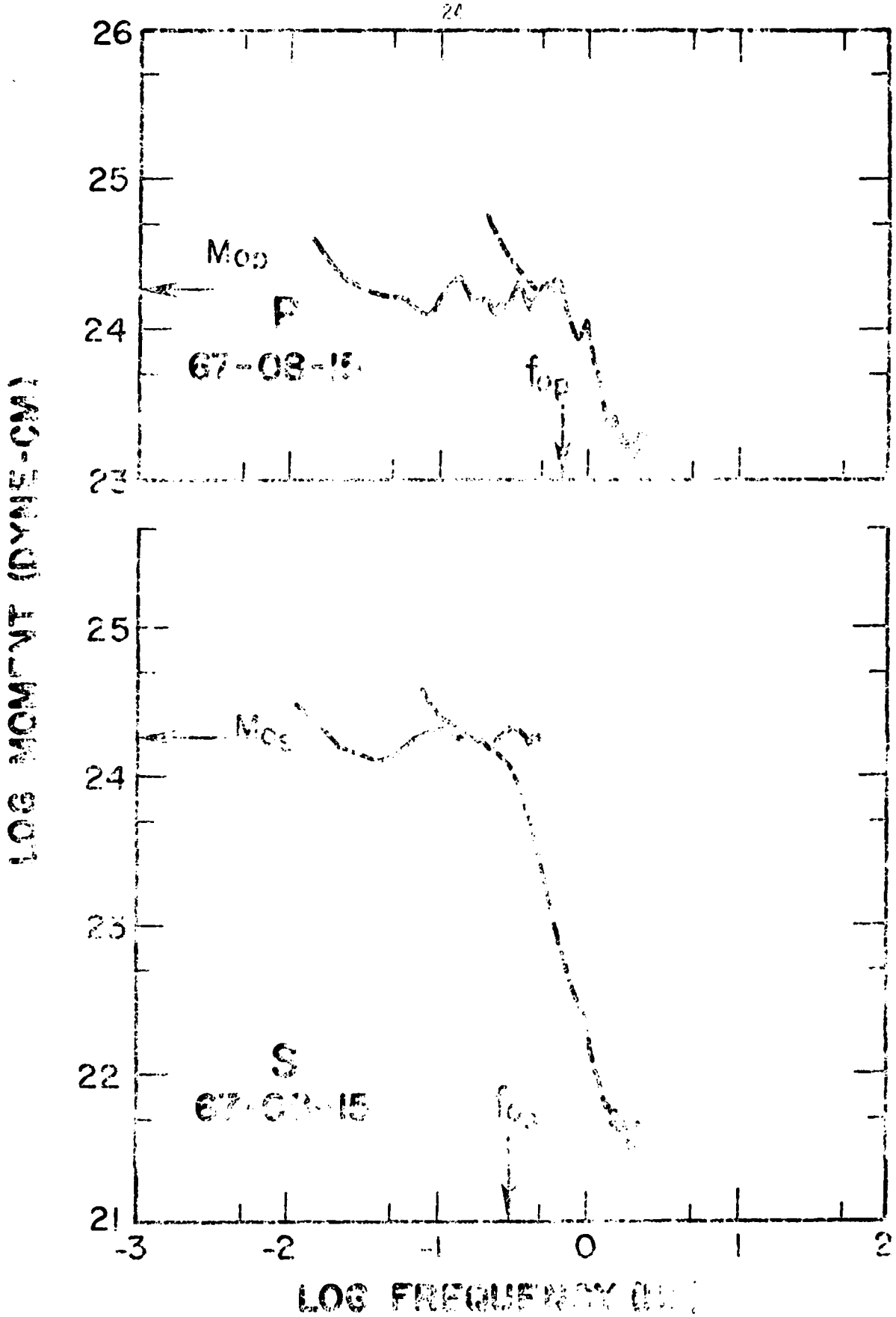

Figure 1.12 Average source spectrum, Tibet event of 67-03-15. S?? from 11, LP? from 3, SP? from 3, LPS from 7.

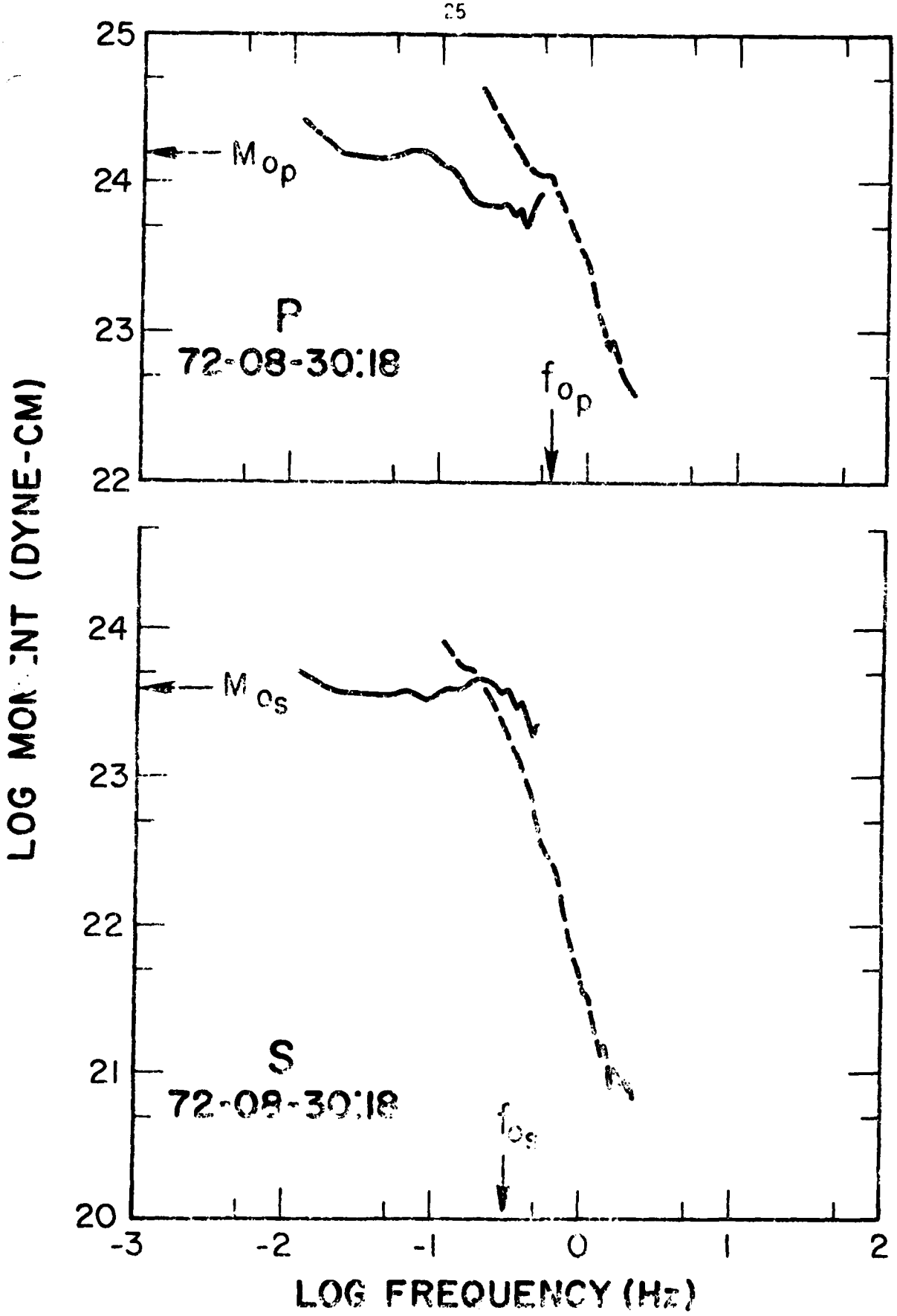

Figure 1.13: Average source spectrum, Tsaidam event of 72-08-30:18. SPP from 7, LPP from 7, SPS from 2, LPS from 5.

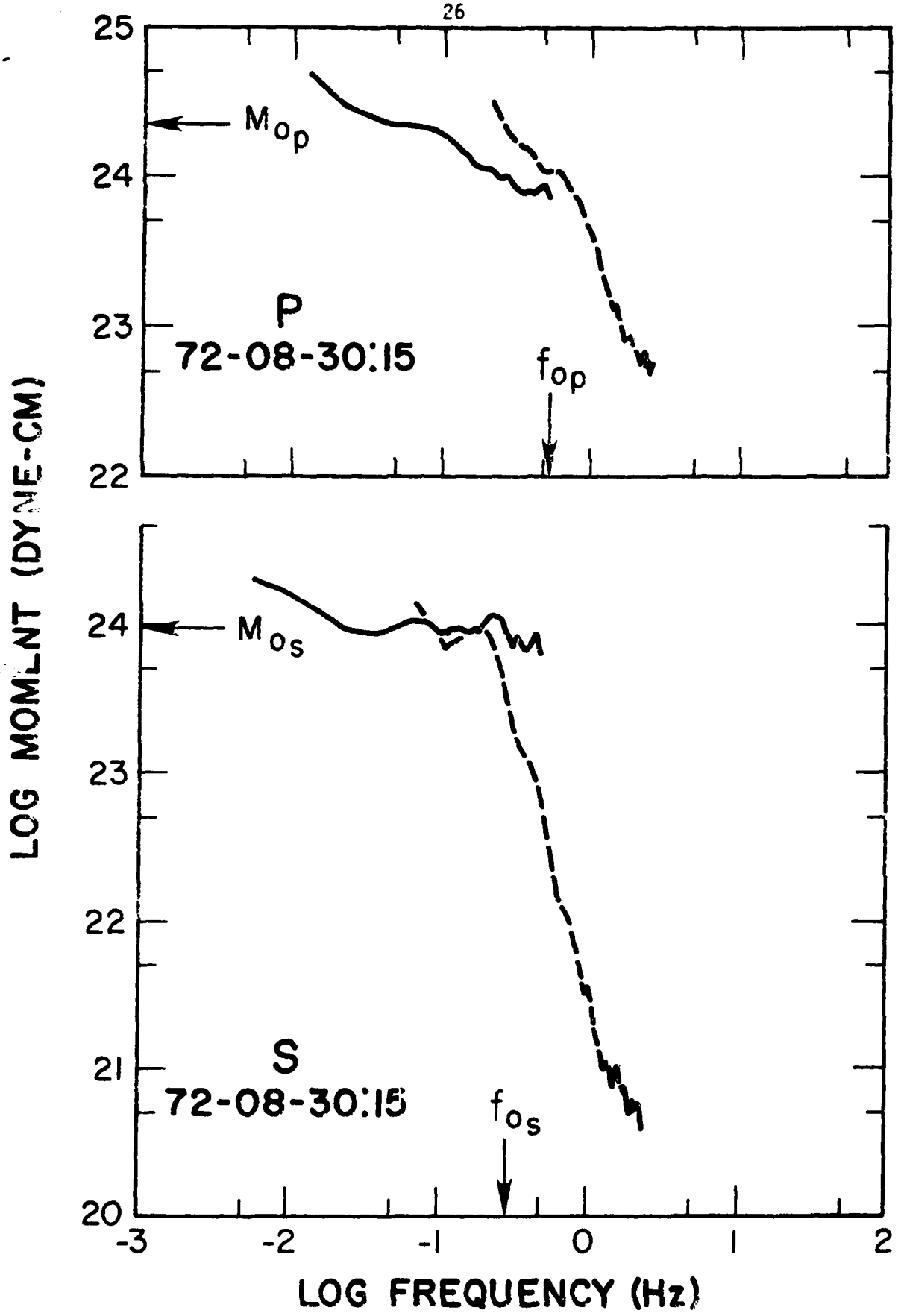

Figure 1.14: Average source spectrum, Tsaidam event of 72-08-30:15. SPP from 7, LPP from 9, SPS from 1, LPS from 10.

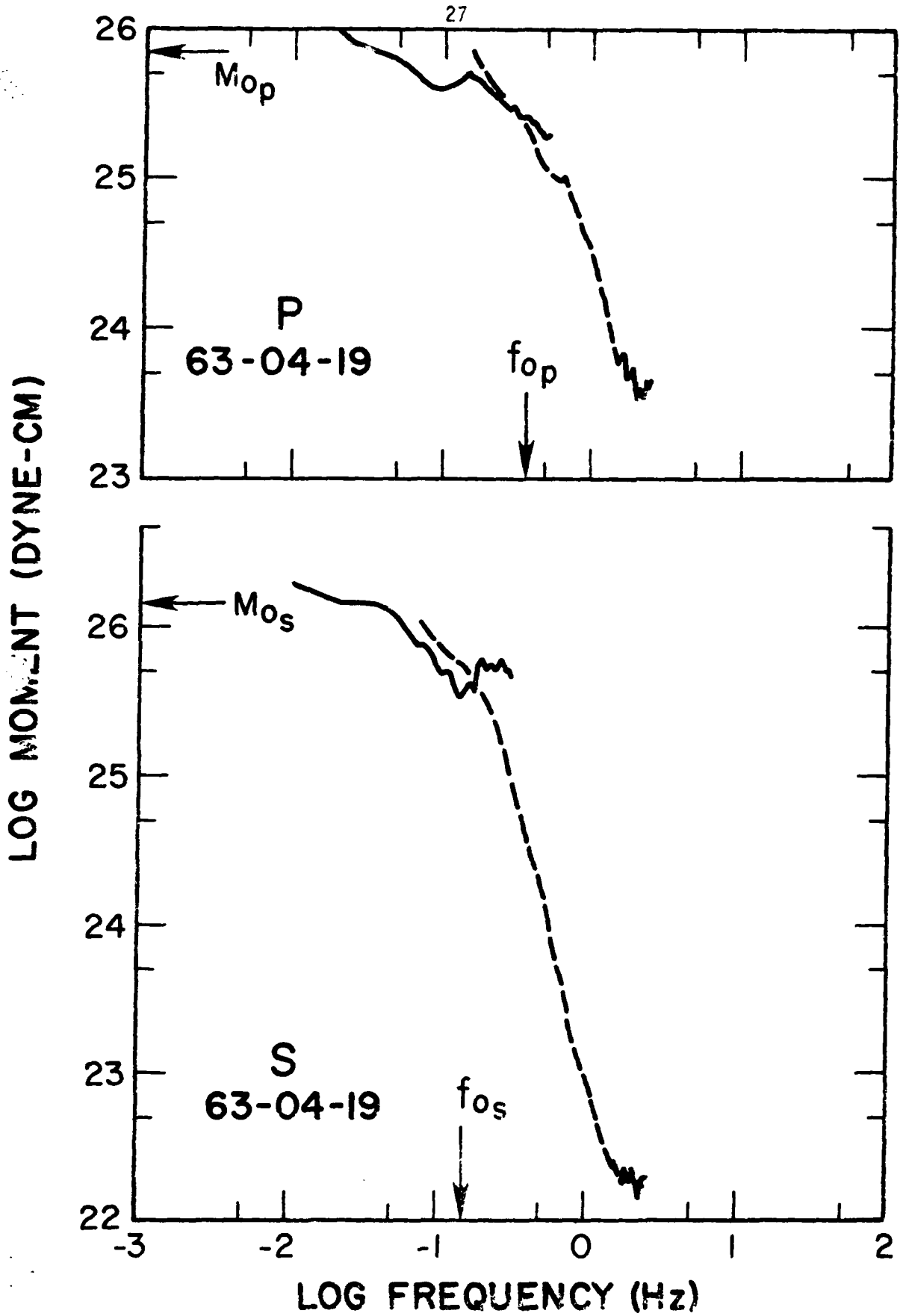

Figure 1.15: Average source spectrum, Tsaidam event of 63-04-19. SPP from 8, [illegible] from 8, SPS from 7, LPS from 7.

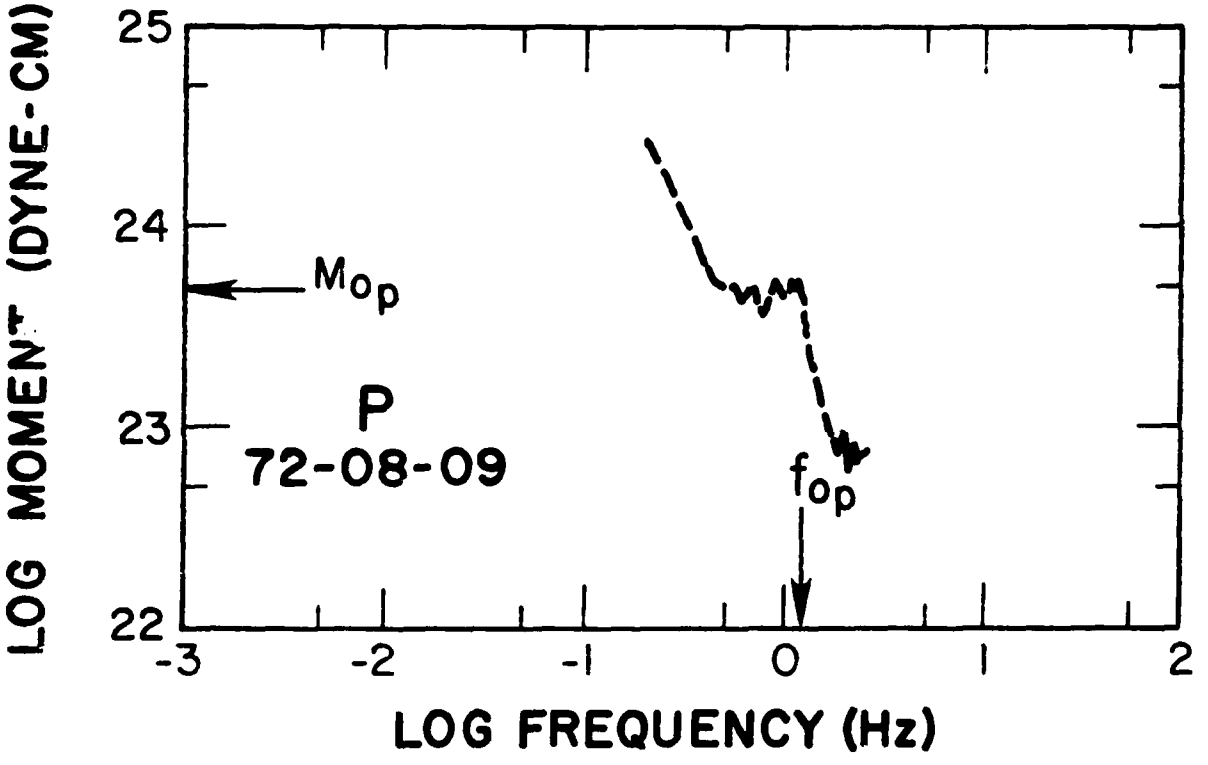

Figure 1.16: Average source spectrum, Lake Baikal event of 72-08-09. SPD from 4.

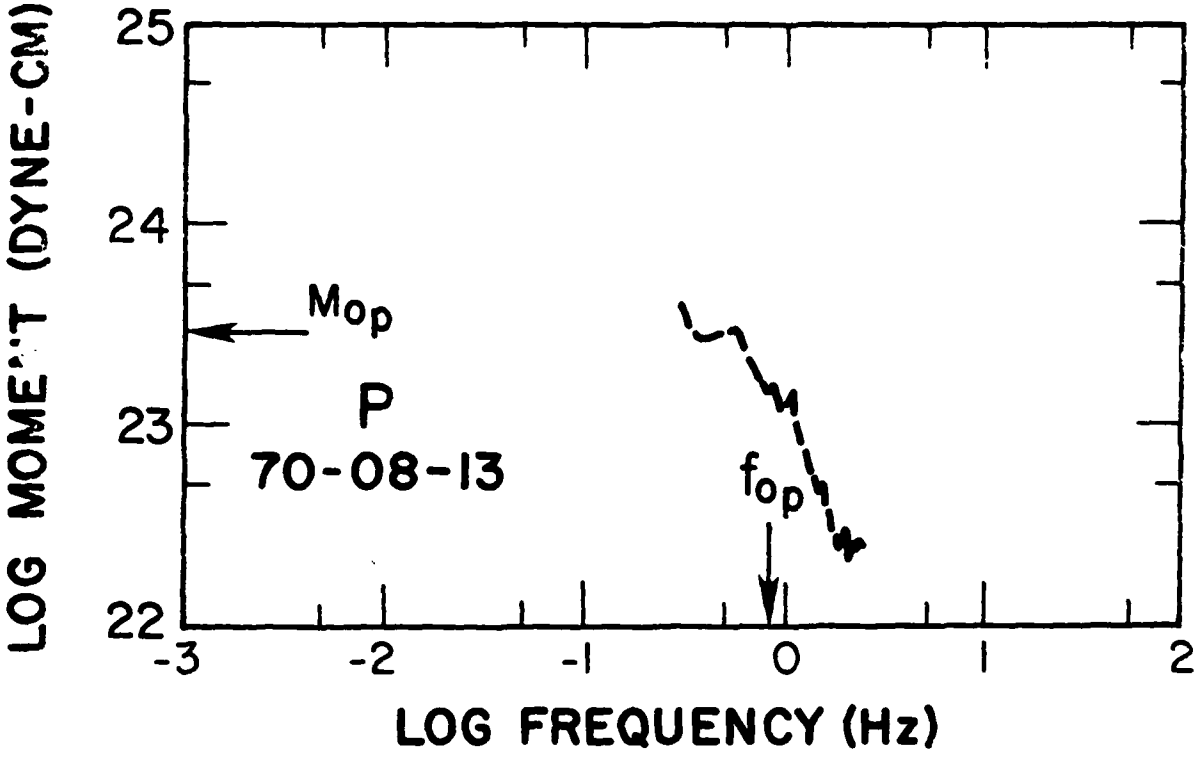

Figure 1.17: Average source spectrum, Lake Baikal event of 70-08-13. SPP from 4.

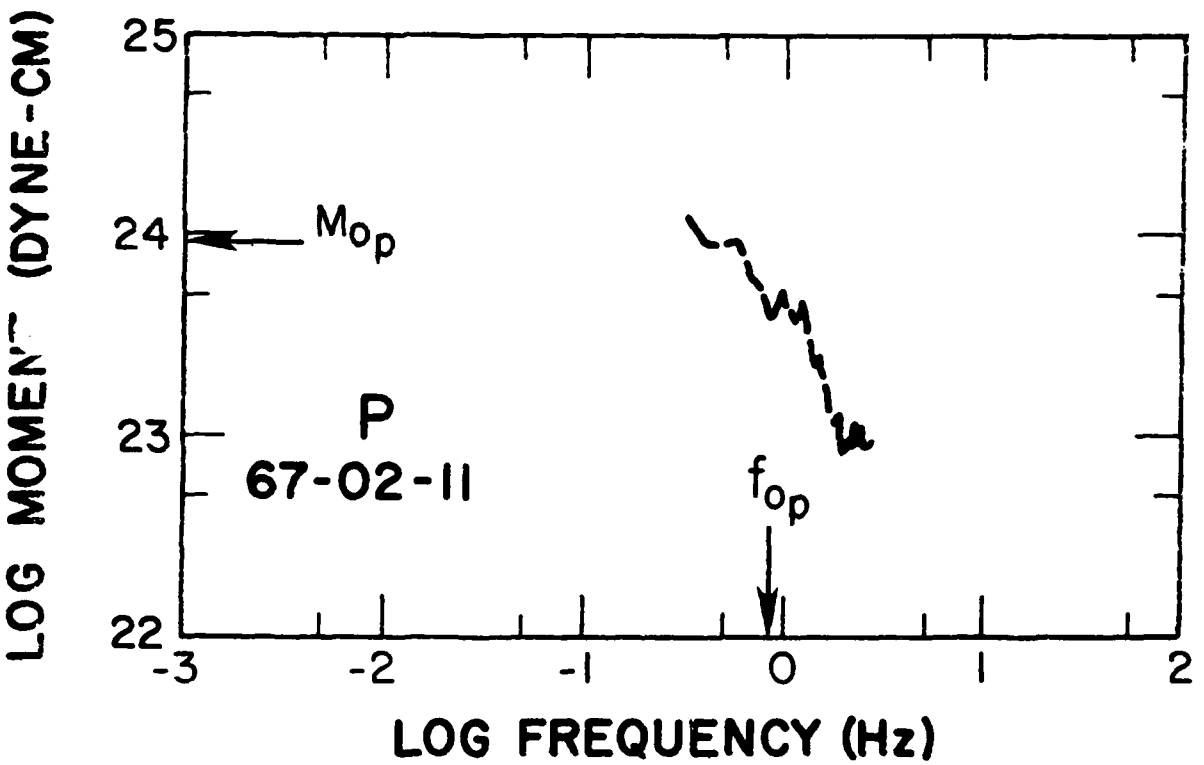

Figure 1.18: Average source spectrum, Lake Baikal event of 67-02-11. SPP from G.

:etan plateau, (3) the block-faulted Tsaidam basin and (4) the Lake Baikal rift zone. Separate and independent estimates were made of short-period P and SH spectra and long-period P and SH spectra. In each case, the best available data were used, whether or not corresponding data was available for the other components.

A crude estimate of the reliability of the spectra is given by the number of stations in each average, as noted in the figure caption. We consider an average of six or more stations to be good, while an average of four or less is questionable. Neither Tsaidam events of 72-08-30 has sufficient short-period S (SPS) data, and those spectra are presented only for comparison.

As mentioned in the introduction, near stations are systematically undercorrected for geometric attenuation. That is, averages dominated by near stations tend to be low. The Tsaidam events of 72-08-30 should have slightly low seismic moments, and, in particular, the SPS spectra are low by a factor of about 2 to 5. The corner frequencies were picked on the LPS spectra.

The spectra are plotted to seismic moment scale, and the choice of moment is shown on each figure by an arrow, and listed in Table 1.1. Moments are plotted vs. earthquake magnitude in Figure 1.19, where the horizontal bars show the difference between body-wave magnitude, m_b, and surface wave magnitude, M_s. The P-wave data fit

$$M_s = -1.7 + 1.3 \log M_o$$

Kanamori and Anderson (1975) find a slope of 2/3, which we cannot possibly fit. The data presented here would, however, fall into the scatter of Kanamori and Anderson's points at the low magnitude end.

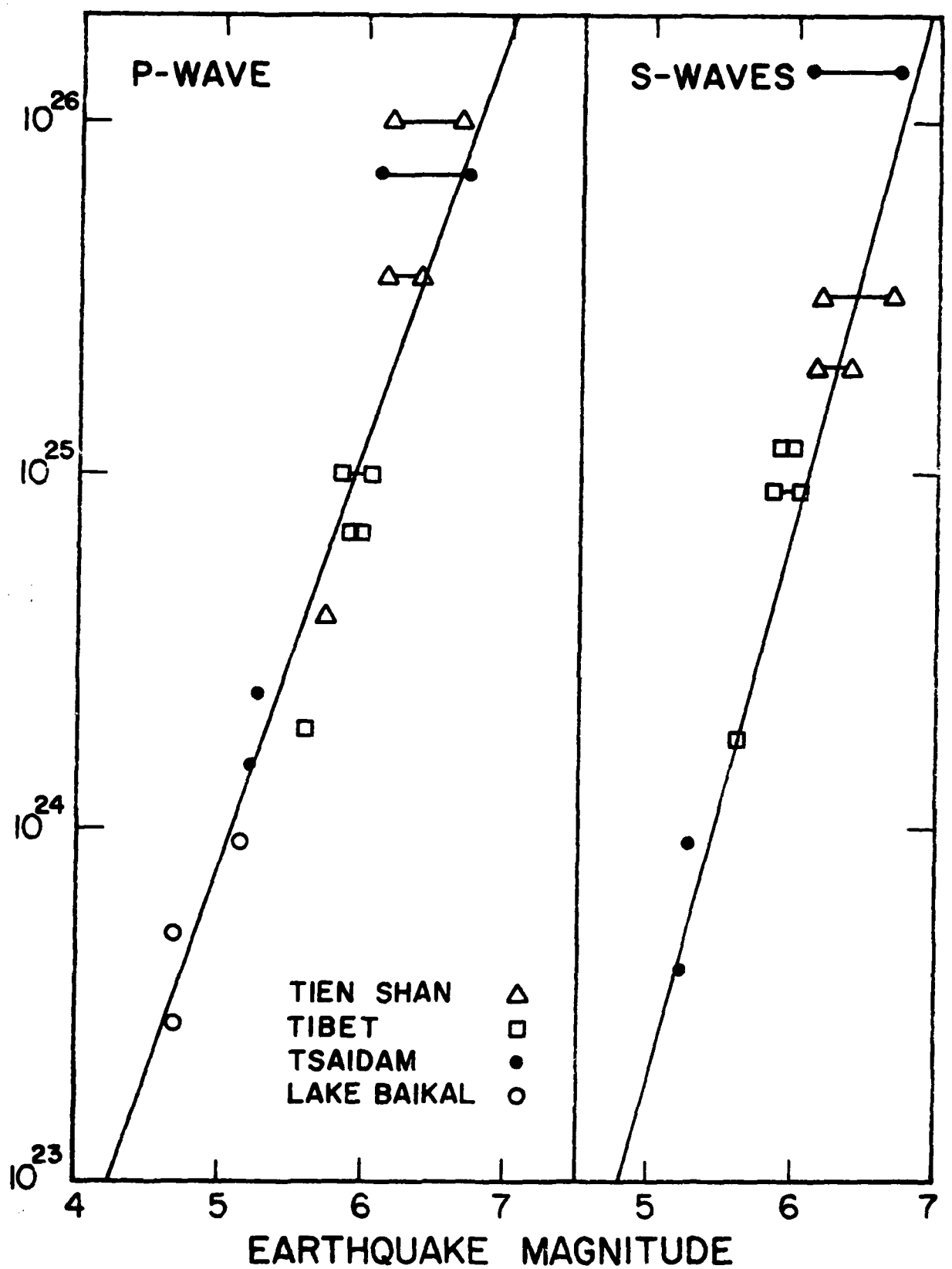

Figure 1.19: Earthquake magnitude vs. seismic moment. When bars are plotted, body wave magnitude, m_b, is on the left, and surface wave magnitude, M_S, is on the right.

TABLE 1.1

	Magnitude		Seismic Moment		Corner Frequency (Hz)	
	m_b	M_s	M_{o_p}	M_{o_s}	f_{o_p}	f_{o_s}
Tien Shan						
72-04-09	5.73	5.43	4.0×10^{24}		.90	
70-06-05	6.17	6.67	1.0×10^{26}	3.2×10^{25}	.26	.26
69-02-11	6.15	6.38	3.6×10^{25}	2.0×10^{25}	.43	.27
Tibet						
71-05-22	5.85	6.04	1.0×10^{25}	9.1×10^{24}	.42	.28
71-04-03	5.91	5.99	6.8×10^{24}	1.2×10^{25}	.59	.27
67-08-15	6.17	6.67	1.9×10^{24}	1.8×10^{24}	.66	.31
Tsaidam						
72-08-30:18	5.22	4.99	1.5×10^{24}	4.0×10^{23}	.60	.30
72-08-30:15	5.26	4.86	2.4×10^{24}	9.1×10^{23}	.51	.30
63-04-19	6.10	6.36	7.2×10^{25}	1.4×10^{26}	.37	.16
Lake Baikal						
72-08-09	4.7		5.0×10^{23}		1.2	
70-08-13	4.7		2.8×10^{23}		.86	
67-02-11	5.15	5.16	9.1×10^{23}		.80	

Note that seismic moments computed from S-wave spectra are smaller than those computed from P-wave spectra with the major exceptions of the Tsaidam event of 63-04-19 and the Tibet event of 71-04-03. The levels are most consistent in Tibet.

Corner frequencies, f_o , are also noted by arrows on spectral plots, listed in Table 1.1 and plotted in Figure 1.20 on an M_o-f_o diagram. f_o is defined as the intersection of a horizontal line through the low-frequency trend with a line through the high-frequency asymptote. Rather than assume a particular high-frequency decay rate, such as ω^{-3} , and fit that slope to the data as well as possible, a best fit line was drawn through the data. And rather than average through the entire short-period spectrum, the quality was judged with respect to the passband of the instrument. The instrument responses are presented in Figure 1.6 to demonstrate that the high-frequency slope should be estimated from frequencies above 0.5 Hz.

If two choices of decay rate could be made, the slope closer to ω^{-3} was chosen. The problem is to distinguish between true slope changes and holes in the spectra. Such questions arose on the P-spectra of 71-05-22, 71-04-03, and 69-02-11.

An examination of the spectra will show that more than half of the P spectra could be interpreted as having more than one corner frequency, while seven of eight S spectra have virtually the same shape. And while P corner frequencies vary with moment, the S corner frequencies are essentially constant. This inconsistency between P and S could possibly be argued in terms of source properties, P-coda contamination of the S wave, PP and PPP contamination of the P wave or other factors, but it more likely represents an insufficient knowledge of the anelastic attenuation operator.

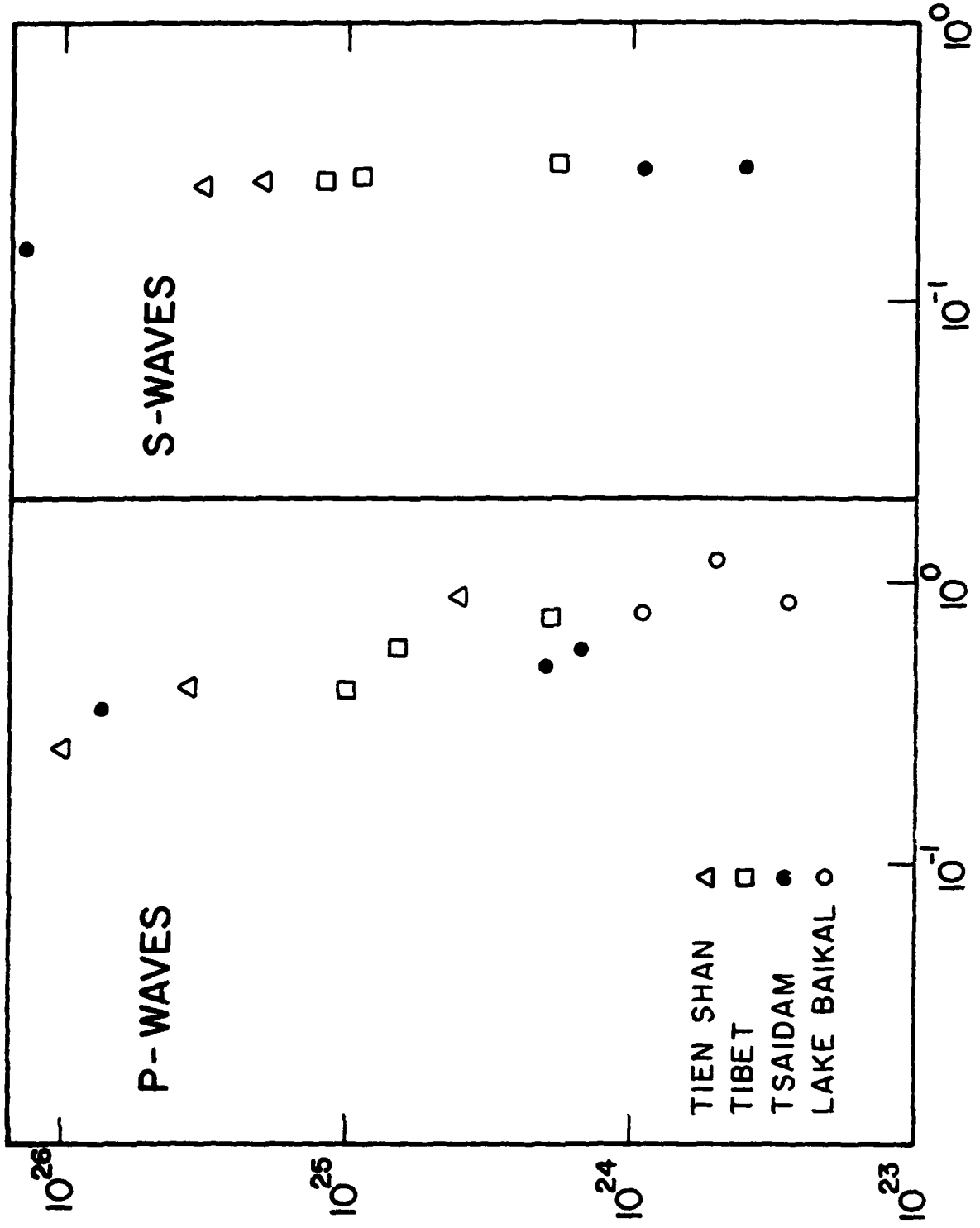

Figure 1.20: Corner frequency, f_0, vs. seismic moment, M_0.

Twelve earthquakes is hardly a statistically significant sample of central Asian seismicity, and these first efforts do not lead to a consistent scaling law relationship. If anything, these events demonstrate the expected heterogeneity of intraplate earthquakes. More data are required to resolve regional characteristics.

References

Anderson, D. L., Latest information from seismic observations, chapter 12 in *The Earth's Mantle* (T. F. Gaskell, Editor), 355-470, Academic Press, 1967.

Biot, M. A., Theory of propagation of elastic waves in a fluid saturated porous solid, Parts I and II, *J. Acoust. Soc. Amer.*, *28*(2), 168-191, 1956.

Kanamori, H. and D. L. Anderson, Theoretical basis of some empirical relations in seismology, *Bull. Seism. Soc. Amer.*, *65*(5), 1073-1095, 1975.

Liu, H. P., D. L. Anderson, and H. Kanamori, Velocity dispersion due to anelasticity, preprint, 1976.

Mason, W. P., *Physical Acoustics and the Properties of Solids*, Van Nostrand Company, Inc., New York, 402 pp., 1958.

Vaisnys, J. R., Propagation of acoustic waves through a system undergoing phase transformations, *J. Geophys. Res.*, *73*(24), 7675-7683, 1968.

2. Focal Parameters from Long-Period Body Waves

W. Gawthrop

Synthesis of Seismograms.

Body wave synthesis has been used in determining focal parameters of a few crustal earthquakes in Asia. Focal depths and focal mechanisms of earthquakes also being studied by analysis of their spectra (Lundquist, this issue) have been the object of this study. Several practical problems have, however, slowed progress in determining these focal parameters. The technique of digitizing long period P-waves in the presence of high noise levels from WWSSN stations to obtain both usable spectra as well as input to body wave synthesis programs has proved to be less than successful. Also, the new program to automatically determine focal parameters by comparing synthetics digitized seismograms has not worked properly to date. The new program searches several trial depths and focal mechanisms, then iterates from the best trial point to obtain the maximum correlation coefficient. Local maxima of correlation, which exist in the scattering of trial focal parameters, confuse the program. Until some control is put into the new program, data must be of exceptionally high quality, with a high signal-to-noise ratio, for a good solution to be obtained. In addition, a means of automatically estimating the errors in the focal parameters still needs to be developed.

The focal parameters obtained from studying seismograms in the time domain through careful analysis are in decreasing order of resolvability, the depth, orientation of the fault planes, seismic moment, duration of faulting, and direction of propagation of rupture. Figure 2.1 shows the first 20 seconds of seven well-distributed seismograms from a thrust earthquake in the Tien Shan province of northwestern China on June 5, 1970. Relative arrival-times of the P, pP, and sP arrivals determine a source depth of

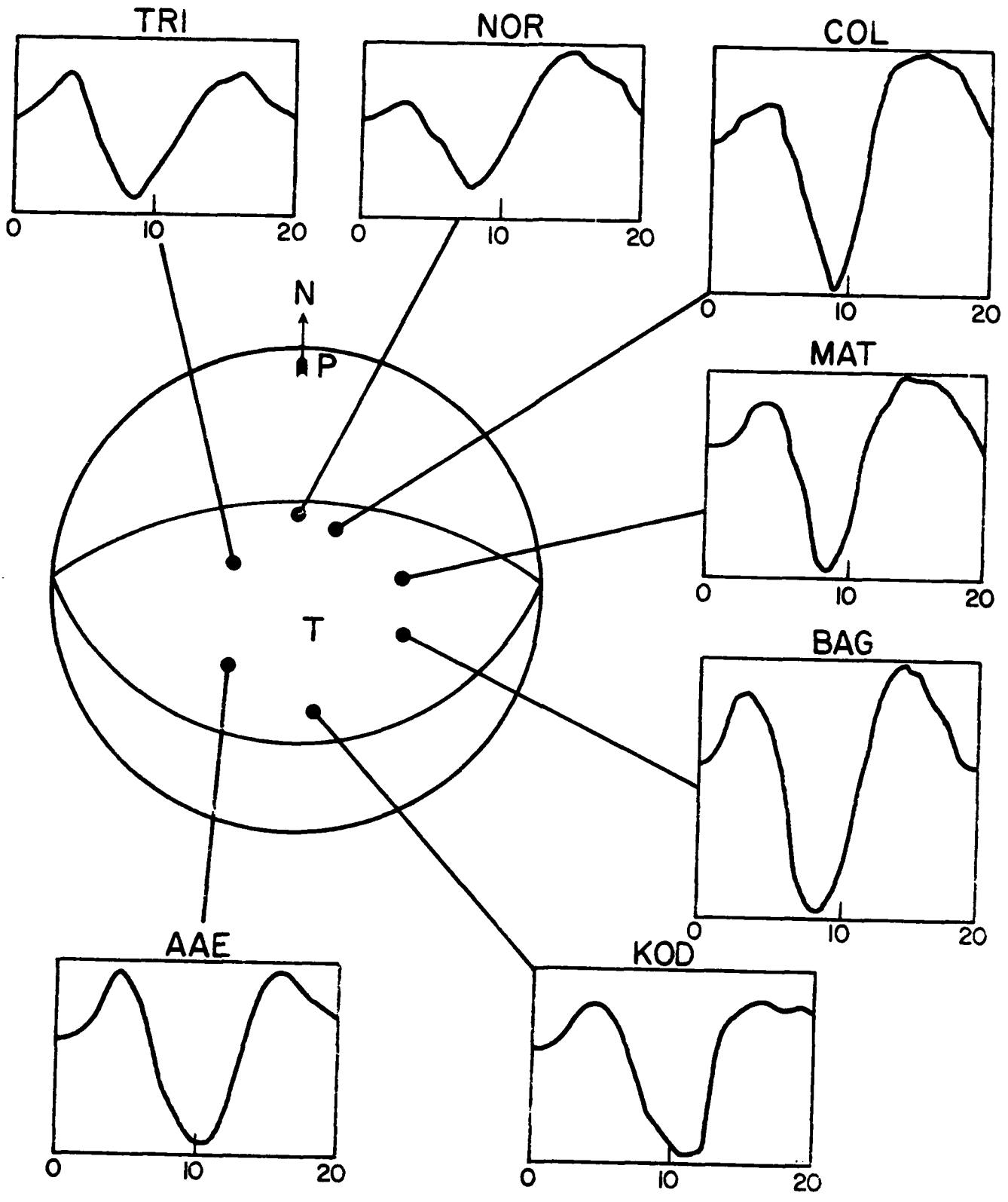

Figure 2.1:

18 kilometers, assuming the earthquake to be a point source and the crust to be of uniform velocity, 6.0 km/sec. Since the shapes of all seven seismograms are quite similar for this event, the focal mechanism can only be determined by careful determination of the relative amplitudes of the peaks corresponding to direct and reflected wave arrivals of maximum energy from the source pulse. The area under the source pulse gives a seismic moment of 2×10^{26} dyne cm.

The duration of the pulse is about 5 seconds, with stations to the east requiring a slightly shorter pulse. This shortening of the pulse to the east is probably due to a doppler shift from an eastward rupturing fault.

Only about 15 seconds of the seismograms can now be accurately matched. This is because most of the early energy comes from the P, pP, and sP waves which have very little dependence on the crustal structures at the source and receiver. Synthesis of wave shapes beyond about 15 seconds can only be considered reliable if we know with confidence, by independent means, the crustal structures in the areas of interest.

Crustal Structure Determination.

A program has been developed to independently determine a crustal velocity structure and Pn velocity in seismically active regions where local networks of seismographs exist. The program utilizes a generalized inversion procedure to simultaneously determine, from P-wave arrival times, hypocenter locations of up to 12 earthquakes and the velocity structure in the local region. A crustal structure with velocity increasing linearly with depth down to a constant velocity upper mantle permits four accurately determined parameters to completely describe the structure. These parameters are the velocity at the surface, the velocity gradient with depth, the depth of the crust, and the velocity at the top of the mantle.

Individual data are weighted according to tne observational error to give the data matrix unit variance for the error analysis. Differently dimensioned parameters are scaled to give each one equal weight in the least squares procedure. A Lagrangian multiplier is incorporated to increase stability during successive iterations. The solution to the equations are given in matrix form as

$$\hat{x} = \left[S(S^T A^T W^T W A S + \varepsilon^2 I)^{-1} S^T A^T W^T W\right]B = GB$$

$$\text{RESOLUTION MATRIX} = GA$$

$$\text{COVARIANCE MATRIX} = G(\text{var}^B)G^T = GG^T$$

where $\hat{x}$ is the calculated change in the model parameters during each iteration, S is the diagonal scaling matrix, A is the matrix of derivatives with respect to the model parameters, W is the diagonal weighting matrix, ε is the Lagrangian multiplier, B is the data matrix, and G is the generalized inversion matrix. Iteration continues until a convergence criterion is satisfied.

Preliminary tests in California and Missouri indicate that the deptn of the crust can be determine to about 25% and the velocity structure of the crust to about 10%. The accuracy improves significantly when known sources, such as explosions, are used, since in many cases, a tradeoff exists between the focal depths of the seismic event and the thickness of tne crust. It is anticipated that the addition of S-wave arrival times to the data set will serve to fix the focal depths and improve the resulting determinations of crustal thickness. It is hoped that the application of this program will improve our understanding of crustal structure so we can better model long-period seismograms for determining focal parameters.

3. The Haicheng Earthquake

Max Wyss

The Haicheng earthquake, M_s = 7.4, occurred on February 4, 1975. It was located in northeastern China (latitude 40.6N, longitude 122.6E). This earthquake is at the present time the only Asian event for which we have detailed information on source parameters derived from geodetic and aftershock studies in the source area. For this reason this event is ideal for testing and calibrating our methods for deriving source parameters for Asian earthquakes. To perform this test we will match the time series and spectra of P-waves, S-waves and surface waves with time series and spectra of theoretical source models.

The Haicheng earthquake is the famous event predicted by Chinese seismologists. Thanks to the prediction effort, geodetic measurements were carried out in the source region before the earthquake. From the repetition of these measurements and aftershocks studies the Chinese derived the source parameters as (Muller, 1976):

Length = 70 km

Width = 17 km (0 to 17 km depth)

Dislocation = 55 cm

Stress drop = 5 bars

The sense of faulting was left lateral along a plane striking N70W, with the propagation mostly towards the northwest.

The first step was to screen the WWSSN data for seismograms with clear signals at distances suitable for analysis. The second step was to digitize these signals. These two tasks are now almost completed. Table 3.1 lists the station for which seismograms have been digitized to date. The first column gives the station abbreviation (WWSSN). The columns headed P, S, R and G give

the number of components digitized at each station for the respective phases. The number 2 in the P column means that a long period and a short period record (usually both z) have been digitized at that station for the P analysis. A number 4 in the S column means that all four horizontal components (long and short period) have been digitized for the S-phase. For the surface waves (R and G) only long period records were digitized.

At the present we are in the process of finishing the third step in the analysis. The Fourier transformation of appropriate windows for all the data digitized. The fourth and final step is just being started. We are generating theoretical spectra and time series with the Archambeau model using the above source parameters as input. The main variable will be the rupture velocity. The objective is to come up with a source model that agrees with the field observations and that generates the far field seismic waves observed. We expect that the results of this study will be ready for publication by the end of the year.

Reference

Muller, P. M. (ed), Proceedings of the Lectures by the Seismological Delegation of the People's Republic of China (translated from Chinese), Pasadena:Jet Propulsion Laboratory, 1976.

TABLE 3.1

Haicheng earthquake, stations and number of components digitized

Station	P	S	R	G	Dist. deg	Azim. deg	Back Azim. deg
ADE	2	2	1	1	77	166	348
ANP				1	15	184	3
ARE			1	2	153	31	336
AQU	2			1	76	314	48
BAG			1	1	24	185	4
BHP				1	127	28	339
BOZ				2	82	35	322
BUL			1	2	106	257	52
CHG			1	2	30	230	36
COL	2			1	54	32	290
COR	2	2	1	2	77	42	314
CTA	1		1	1	64	155	340
DAL			2	1	98	33	331
ESK	2	4	1	2	74	331	40
GIE				2	130	45	327
GUA	2	3	1		33	138	328
HNR	2				61	137	328
IST	2	4		2	67	305	56
JCT			1	1	99	36	329
KBS	2				54	347	61
KEV	2			1	54	335	69
KIP	2	1	1	2	69	80	307
LEM				1	49	200	15
MSH	2	4		2	49	286	66
NIL				1	40	276	66
NUR	2				59	325	61
SHA			1		104	27	334
SNG	1		1		39	216	37
STU	2	2			73	321	47
TAB	1				57	294	62
TUC			1	2	92	45	322
VAL	2	4		2	79	333	35
TOTAL	33	27	16	36			

SECURITY CLASSIFICATION OF THIS PAGE (When Data Entered)

REPORT DOCUMENTATION PAGE		READ INSTRUCTIONS BEFORE COMPLETING FORM
1. REPORT NUMBER Semi-annual technical report no.4	2. GOVT ACCESSION NO.	3. RECIPIENT'S CATALOG NUMBER
4. TITLE (and Subtitle) Seismic Wave Propagation and Earthquake Characteristics in Asia		5. TYPE OF REPORT & PERIOD COVERED Semi-Annual Technical Report 1 May - 30 October 1976 6. PERFORMING ORG. REPORT NUMBER
7. AUTHOR(s) C. Kisslinger, E. R. Engdahl, M. Wyss, W. Gawthrop, G. Lundquist		8. CONTRACT OR GRANT NUMBER(s) AFOSR-75-2775
9. PERFORMING ORGANIZATION NAME AND ADDRESS CIRES University of Colorado Boulder, Colorado 80309		10. PROGRAM ELEMENT, PROJECT, TASK AREA & WORK UNIT NUMBERS ARPA Order 1827 Program Code 5F10 Program Element 62701E
11. CONTROLLING OFFICE NAME AND ADDRESS Advanced Research Projects Agency/NMR 1400 Wilson Boulevard Arlington, Virginia 22209		12. REPORT DATE 31 October 1976 13. NUMBER OF PAGES 44
14. MONITORING AGENCY NAME & ADDRESS(if different from Controlling Office) Air Force Office of Scientific Research/NP Bolling Air Force Base, Bldg. 410 Washington, D. C. 20332		15. SECURITY CLASS. (of this report) UNCLASSIFIED 15a. DECLASSIFICATION/DOWNGRADING SCHEDULE

16. DISTRIBUTION STATEMENT (of this Report)

Approved for public release; distribution unlimited.

17. DISTRIBUTION STATEMENT (of the abstract entered in Block 20, if different from Report)

18. SUPPLEMENTARY NOTES

19. KEY WORDS (Continue on reverse side if necessary and identify by block number)

source spectra
inelastic attenuation
corner frequencies
Haicheng earthquake
focal depth
crustal modelling

20. ABSTRACT (Continue on reverse side if necessary and identify by block number)

A relaxation mdoel of attenuation leading to a frequency-dependent Q has been incorporated into the procedure for computing seismic source spectra. Results for P and S-wave spectra from 12 central Asian earthquakes show a dependence of corner frequency on moment for P-waves, but not for S. Data from the Haicheng, China, earthquake have been assembled to provide a calibration of techniques of determining source properties of Asian earthquakes from teleseismic data. Further work on the procedure for fixing focal parameters on the basis of long-period body wave properties includes an attempt to automate

DD FORM 1 JAN 73 1473 EDITION OF 1 NOV 65 IS OBSOLETE

UNCLASSIFIED

SECURITY CLASSIFICATION OF THIS PAGE (When Data Entered)

20.

the procedure and development of a program for determining the parameters of a selected crustal model when local network data are available.